

RESEARCH

Open Access



Danshenol B alleviates central post-stroke pain by regulating the PIK3CG/NLRP3 signaling pathway

Panyang Li^{1†}, Linna Yu^{5†}, Jinzhong Yao⁴, Tingting Zhao¹ and Sen Zhao^{2,3*} 

Abstract

Background Central post-stroke pain (CPSP) is a debilitating neuropathic condition that significantly impairs quality of life and is challenging to manage. *Salvia miltiorrhiza* (Danshen), a traditional Chinese herb, has demonstrated efficacy against neuropathic pain, but its active analgesic components and underlying mechanisms remain unclear. This study investigated the therapeutic potential of Danshenol B, an active component of Danshen, in a CPSP mouse model, focusing on its mechanism of action via the phosphatidylinositol-4,5-bisphosphate 3-kinase catalytic subunit gamma isoform (PIK3CG)/NLR family pyrin domain-containing protein 3 (NLRP3) signaling pathway.

Methods A CPSP model was established in mice, and RNA sequencing of the ipsilateral ventral posterolateral thalamic nucleus/ventral posteromedial thalamic nucleus (VPL/VPM) was performed to identify differentially expressed genes (DEGs). Network pharmacology analysis linked these DEGs to known Danshen components, and molecular docking of 42 Danshen constituents was conducted to identify strong ligand-target interactions. Danshenol B was then administered (5, 10, 50 mg/kg) to CPSP mice to evaluate its analgesic effects, and thalamic PIK3CG and NLRP3 protein levels were measured to assess pathway involvement. Additionally, PIK3CG and NLRP3 expression were manipulated (via overexpression or knockdown) to determine their roles in CPSP and their regulatory relationship.

Results In the CPSP model, 409 DEGs were identified in the ipsilateral VPL/VPM. Network pharmacology revealed 21 Danshen-derived compounds potentially targeting 11 of these DEGs. Molecular docking highlighted Danshenol B as a top candidate, showing strong binding (-9.127 kcal/mol) to PIK3CG. In CPSP mice, Danshenol B (50 mg/kg) significantly alleviated CPSP and suppressed the PIK3CG/NLRP3 pathway. The overexpression of PIK3CG increased NLRP3 and negated the effects of Danshenol B, whereas its knockdown alleviated CPSP and reduced NLRP3. Notably, simultaneous overexpression of NLRP3 attenuated the analgesic effects induced by PIK3CG knockdown, further confirming that NLRP3 functions downstream of PIK3CG in mediating CPSP.

Conclusions Danshenol B alleviates CPSP in mice by suppressing the PIK3CG/NLRP3 signaling pathway, elucidating its analgesic mechanism and highlighting its potential as a novel therapeutic candidate for CPSP.

[†]Panyang Li and Linna Yu contributed equally to this work.

*Correspondence:
Sen Zhao
zhaosen90@163.com

Full list of author information is available at the end of the article



© The Author(s) 2025. **Open Access** This article is licensed under a Creative Commons Attribution-NonCommercial-NoDerivatives 4.0 International License, which permits any non-commercial use, sharing, distribution and reproduction in any medium or format, as long as you give appropriate credit to the original author(s) and the source, provide a link to the Creative Commons licence, and indicate if you modified the licensed material. You do not have permission under this licence to share adapted material derived from this article or parts of it. The images or other third party material in this article are included in the article's Creative Commons licence, unless indicated otherwise in a credit line to the material. If material is not included in the article's Creative Commons licence and your intended use is not permitted by statutory regulation or exceeds the permitted use, you will need to obtain permission directly from the copyright holder. To view a copy of this licence, visit <http://creativecommons.org/licenses/by-nc-nd/4.0/>.

Keywords Central post-stroke pain, *Salvia miltiorrhiza*, Danshen, PIK3CG, NLRP3

Background

CPSP is a type of neuropathic pain directly associated with stroke lesions that occurs in both ischemic and hemorrhagic stroke patients [1]. CPSP affects approximately 1–35% of stroke survivors, with markedly higher incidences reported when lesions involve critical regions such as the medulla or thalamus, where prevalence rates can exceed 24% and 50%, respectively [2, 3]. CPSP symptoms may emerge immediately after stroke or develop progressively, typically between one and twelve months [4]. Furthermore, approximately 35–51% of patients experience evoked pain, often triggered by mechanical allodynia or cold hyperalgesia [5]. In basic research, CPSP models are most commonly established by injecting collagenase or autologous blood into the brain [6, 7]. Studies have shown that the pathophysiology of CPSP is complex, involving inflammatory responses [2, 8], microglial activation [6], apoptosis, neurovascular and blood-brain barrier disruptions [9], oxidative stress [10], and free radical production [11]. Current treatment options in Western medicine for CPSP include pharmacological agents, such as amitriptyline, lamotrigine, and gabapentin, as well as physical interventions including motor cortex stimulation, spinal cord stimulation, repetitive transcranial magnetic stimulation, and transcranial direct current stimulation [12–14]. Despite these interventions, many patients continue to experience suboptimal outcomes. Traditional Chinese medicine (TCM) has gained increasing attention due to its favorable safety profile and widespread acceptance in clinical practice.

As a TCM, Danshen exhibits significant anti-inflammatory, antioxidant, and antiapoptotic properties, which are directly relevant to the pathogenesis of CPSP [15]. Most research on Danshen in the context of stroke has focused on ischemic stroke, owing to its well-established efficacy in promoting blood circulation and removing stasis. In contrast, its application in hemorrhagic stroke remains underexplored, largely due to the prevailing concern that blood-activating and stasis-resolving herbs may exacerbate bleeding. However, a 2019 randomized trial involving 537 hemorrhagic stroke patients published in *The Lancet* reported that antithrombotic therapy did not increase the risk of recurrent bleeding [16], suggesting that such concerns may be overstated. Emerging evidence also indicates that compound Danshen preparations can alleviate pain through mechanisms involving signal transduction pathways, the endocrine system, and the nervous system [17]. Thus, exploring the role of individual Danshen constituents in the context of cerebral hemorrhage and pain may yield valuable insights. In 1997, Tezuka et al. isolated a bioactive compound, Danshenol

B ($C_{22}H_{26}O_4$), from the methanol extract of *Salvia miltiorrhiza* Bunge, which exhibited strong aldose reductase (AR) inhibitory activity [18]. Despite this, research on Danshenol B remains limited, and its pharmacological effects are not well characterized. Although no studies to date have examined analgesic potential or mechanisms of Danshenol B, it is worth noting that AR plays a key role in the development of sensory abnormalities in diabetic neuropathy [19]. Additionally, data from the Traditional Chinese Medicine Systems Pharmacology (TCMSP) platform suggest that Danshenol B may target the Mu-type opioid receptor, highlighting its potential relevance for pain management. Collectively, these findings support the hypothesis that Danshenol B may possess therapeutic value in the treatment of CPSP.

Danshen targets numerous proteins, and the pathophysiology of stroke involves a wide range of molecular pathways. One such key target is PIK3CG (also known as PI3K γ), a catalytic subunit of phosphoinositide 3-kinase that plays a pivotal role in regulating inflammation and oxidative stress. PIK3CG has been implicated in various disease states, including autoimmune disorders and multiple myeloma [20–22]. Recent studies have demonstrated that PIK3CG is significantly upregulated in ischemic stroke lesions, where it activates microglia and astrocytes, contributing to neuroinflammation and stroke progression [23, 24]. Knockdown of PIK3CG has been shown to reduce blood–brain barrier permeability and decreases infarct volume [25]. Furthermore, PIK3CG-mediated activation of the Akt signaling pathway has been associated with bone cancer pain, suggesting that PIK3CG may play a role in both stroke and pain pathophysiology [26]. NLRP3, which is involved in inflammasomes and pyroptosis [27, 28], is implicated in conditions such as depression [29], arthritis [30], and atherosclerosis [31]. Inhibition of the HIF-1 α /NLRP3 signaling pathway has been shown to alleviate pain, anxiety, and depression in hemorrhagic stroke patients [6]. NLRP3 interacts with the Stimulator of Interferon Genes (STING) protein to promote microglial pyroptosis during ischemic stroke [32]. Additionally, certain TCMs provide neuroprotection by inhibiting NLRP3 during stroke [33]. Collectively, these findings highlight the critical roles of both PIK3CG and NLRP3 in the molecular mechanisms underlying stroke and pain, and support the rationale for investigating the PIK3CG/NLRP3 axis as a therapeutic target in CPSP.

In this study, we established a mouse model of CPSP and performed transcriptomic sequencing to investigate gene expression changes associated with the condition. Using network pharmacology analysis, we identified

key active components of Danshen and their potential molecular targets relevant to CPSP. Among these, Danshenol B—a major bioactive compound—was selected for further evaluation. We assessed its therapeutic efficacy through oral administration in CPSP mice. Additionally, we explored the underlying molecular mechanisms by which Danshenol B exerts its analgesic effects, with a particular focus on the regulation of the PIK3CG/NLRP3 signaling pathway. Based on these investigations, we hypothesize that Danshenol B alleviates CPSP by inhibiting the PIK3CG/NLRP3 signaling pathway, offering a novel therapeutic strategy for post-stroke pain management.

Methods

Animal preparation

Male C57BL/6J mice, weighing 25–30 g each, were obtained from Beijing Vital River, China. The mice were housed under a 12-hour light–dark cycle at a temperature of $24\text{ }^{\circ}\text{C} \pm 1\text{ }^{\circ}\text{C}$ and humidity levels of 40–60%, with ad libitum access to food and water. The mice were acclimated for a minimum of 7 days before the commencement of the experiments. All animal care procedures were approved by the Zhengzhou University Animal Care and Use Committee and complied with the International Association for the Study of Pain guidelines. Ethical approval was obtained from the Zhengzhou University Ethics Committee (Approval No. ZZUIRB2024-191).

Intracranial injection

After the mouse was anesthetized with 3% isoflurane (RWD Life Technology Co., Ltd., China), it was placed in a stereotaxic apparatus (Harvard Apparatus, Cambridge, MA), the head was secured with ear bars, and anesthesia was maintained with 1.5% isoflurane. The skin was disinfected, an incision was made, and hydrogen peroxide was used to remove the periosteum. To induce central post-stroke pain, as previously described [7], a glass electrode-tipped microliter syringe (7001KH, Hamilton, USA) was used to inject collagenase IV (Coll) (0.01 U/10 nL, Sigma–Aldrich, St. Louis, MO, USA) into the right VPL/VPM at the following coordinates: lateral: 1.52 mm, bregma: -1.67 mm, depth: -3.6 mm. The control group was injected with an equal volume of saline. The injection was performed over 10 min at a constant rate. After injection, the syringe was retracted by 0.1 mm, held in place for an additional 10 min to prevent reflux, and then slowly withdrawn.

For mechanistic studies, lentiviral particles encoding either a PIK3CG overexpression construct (LV-pik3cg-OE, SC-424436-LAC, Santa Cruz Biotechnology, CA, USA), PIK3CG shRNA (sh-pik3cg, SC-39130-V, Santa Cruz Biotechnology), NLRP3 overexpression construct (LV-NLRP3-OE, SC-432122-LAC, Santa Cruz

Biotechnology), Control Lentiviral Activation Particles (LV-NC, SC-437282, Santa Cruz Biotechnology) or Control CRISPR/Cas9 Plasmid (sh-NC, SC-418922, Santa Cruz Biotechnology) were injected into the same stereotaxic coordinates in separate groups of CPSP mice. These injections were administered after CPSP model establishment to modulate PIK3CG or NLRP3 expression *in vivo* and to investigate their roles in the analgesic effects of Danshenol B. Following each injection, the skull was moistened with saline, the incision was sutured, and the wound was disinfected with iodine tincture. The mice were then placed in a $36\text{ }^{\circ}\text{C}$ recovery chamber for post-operative monitoring and care. The rationale for PIK3CG overexpression was to determine whether it is functionally required for the analgesic effect of Danshenol B.

Administration of Danshenol B

For drug administration, Danshenol B (purity of 99%, HY-122963, MCE, USA, CAS: 189308-09-6) was diluted in PBS. A 6-gauge gavage needle was used to aspirate the diluted Danshenol B (for the control group, the same volume of PBS was used). Gently grasp the mouse and fix its head with the mouse facing upward. The gavage needle was inserted from the upper jaw and gently pushed inward. Once the needle reaches halfway through the needle, it feels the absence of resistance; then, the drug is injected, and the gavage needle is withdrawn. The drug was administered once daily for 21 consecutive days.

Modified neurological severity score

The modified neurological severity score (mNSS) was used to assess neurological function [34]. The evaluation included measurements of motor skills, sensory perception, balance, and reflexes, with scores ranging from 0 to 18. Lower scores indicate better neurological status, whereas higher scores reflect more severe deficits. Detailed scoring criteria are provided in Supplementary Table S1.

Behavioral tests

Von Frey testing

Mechanical sensitivity was assessed via von Frey filaments (Stoelting, Wood Dale, IL, USA) with forces of 0.07 g and 0.4 g [35]. Paw withdrawal frequency (PWF) was measured by applying von Frey filaments to the central region of the plantar surface of the hind paw. The number of paw withdrawals was recorded over 10 trials to quantify sensitivity to mechanical stimuli.

Thermal hyperalgesia test

Thermal hyperalgesia was measured by recording the paw withdrawal latency (PWL) in response to a heat source. The mice were placed on a raised glass platform, and a radiant heat source was directed onto the plantar

surface of the hind paw through the glass plate. The withdrawal time of the hind paw following radiant heat application was recorded. Each hind paw was tested individually, with a 10-minute interval between tests.

Cold plate assay

The animals were placed on a plate precooled to 0 °C, and a timer was started immediately upon placement. The timer was stopped when the animals exhibited behaviors such as paw lifting, flinching, or guarding. The duration from initial placement to the observed flinch was recorded as the PWL in response to painful cold stimuli.

Nissl staining

Nissl staining was used to visualize Nissl bodies within the neuronal cytoplasm. Tissue sections were immersed in Nissl staining solution (Beyotime, Shanghai, China) for 10 min at room temperature. After staining, the sections were washed twice with distilled water and then rinsed with 70% ethanol to remove excess dye. Images of stained Nissl bodies were acquired using an Olympus DP80 microscope (Olympus, Japan). Image analysis and processing were conducted using ImageJ software (version 2.9.0; National Institutes of Health, Bethesda, MD, USA).

Tissue collection and RNA extraction

The study used two groups of mice, each comprising three biological replicates. Right-sided VPL/VPM tissues were separately extracted from each mouse. Each sample consisted of pooled tissues from three mice, resulting in nine mice per treatment group. Following the manufacturer's guidelines, total RNA was isolated via a miRNeasy kit, which includes on-column genomic DNA digestion (Qiagen, Valencia, CA, USA). The RNeasy Micro Kit (Qiagen) was used for RNA purification, and concentrations were measured with a NanoDrop 2000 Spectrophotometer (Thermo Scientific, Wilmington, DE, USA). Sample quality was assessed via A260/280 ratios (1.97–2.08) with an Agilent 2100 Bioanalyzer (Agilent Technologies, Santa Clara, CA).

RNA sequencing

Total RNA (1.0 µg per sample) was subjected to rRNA depletion via the Ribo-Zero rRNA Removal Kit (Human/Mouse/Rat; Illumina, San Diego, CA, USA). Eukaryotic mRNA was enriched via magnetic beads conjugated with oligo (dT) and fragmented randomly with fragmentation buffer. First-strand cDNA was synthesized from mRNA via random hexamer primers (Thermo Fisher Scientific, USA). A mixture of buffer, dNTPs, RNase H, and DNA polymerase I was subsequently added to synthesize second-strand cDNA, which was then purified via AMPure XP beads (Beckman Coulter, Brea, CA). The purified double-stranded cDNA was processed for end repair,

A-tailing, and adapter ligation. This was followed by size selection via AMPure XP beads and enrichment of the cDNA library via PCR. RNA sequencing was performed on the Illumina Nova6000 platform (Illumina, San Diego, USA) using 2 × 150 bp paired-end reads, resulting in a minimum of 20 million reads per sample. Over 21.08 million reads were obtained in each group, ranging from 21.08 to 27.47 million in the Saline group and 22.55 to 27.03 million in the Coll group.

After trimming, the reads were aligned to the ENSEMBL reference mouse genome (GRCm38.95). Mapped reads distribution across genomic regions was visualized using HISAT2 (version 2.2.1) with the parameters `--dta -p 6 --max` [36]. The aligned reads were classified into exonic, intronic, and intergenic regions. Supplementary Fig. 1A shows the distribution of these categories in the Saline and Coll groups from the VPL/VPM. The overall dispersion of the samples in each group was similar (Supplementary Fig. 1B). The Pearson correlation coefficient between samples within each group was approximately 1 (Supplementary Fig. 1C). Principal component analysis revealed a clear separation between the Saline and Coll groups along PC1, which explained 96.4% of the total variance, indicating robust transcriptional reprogramming in the ipsilateral VPL/VPM 14 days after collagenase injection (Supplementary Fig. 1D).

Gene expression levels were quantified using featureCounts and analyzed with DESeq2 (v1.30.1) for differential expression between the Saline and Collagenase groups [37, 38]. Genes with a fold change ≥ 2 and an adjusted *P*-value (FDR) < 0.05 were considered significantly differentially expressed. Identified DEGs were classified as upregulated or downregulated based on their expression trends.

The RNA-seq data were uploaded with the Gene Expression Omnibus accession number GSE281041.

Functional enrichment analysis of differentially expressed genes

For functional analysis, approximately 409 DEGs ($P < 0.05$, fold change ≥ 2) from the VPL/VPM were categorized using Kyoto Encyclopedia of Genes and Genomes (KEGG) pathway and Gene Ontology (GO) analyses via clusterProfiler (version 3.10.1, minGSSize = 1, maxGSSize = 10000, pAdjustMethod = "fdr"). Genetic regulatory networks were elucidated by organizing hierarchical categories into biological processes (BP), molecular functions (MF), and cellular components (CC). Gene set enrichment analysis (GSEA) was conducted via clusterProfiler (v3.10.1, nPerm = 1000). The GSEA utilized KEGG pathways and GO terms from the BP, CC, and MF categories as gene sets of interest, with the log₂FC of each differential group serving as the ranked background gene set.

Protein–protein interaction (PPI) network construction

To better understand the functional relationships among DEGs, interactions among significant DEGs in the VPL/VPM were predicted using the STRING database (version 12.0). Using Cytoscape (version 3.10.1), a network was constructed from the top 50 DEGs exhibiting the strongest correlations. The Centiscape plugin was used to determine the degree of connection for each node, which was represented by the node size. Nodes are color-coded red for upregulated genes and blue for downregulated genes.

Collection of danshen targets

We used the TCMSP (version 2.3) database to identify Danshen's active constituents, selecting those with oral bioavailability $\geq 30\%$ and drug likeness ≥ 0.183 . We then retrieved the SMILES codes for 42 Danshen components from the PubChem database (<https://pubchem.ncbi.nlm.nih.gov/>, accessed on 14 July 2024). We uploaded these SMILES codes to the SwissTargetPrediction database (<http://www.swisstargetprediction.ch/>, accessed on 14 July 2024) to identify molecular targets. We cross-referenced these targets with DEGs to pinpoint Danshen's therapeutic targets for CPSP treatment and visualized the results with a Venn diagram (<https://www.bioinformatics.com.cn/>). The 11 identified therapeutic targets were uploaded to STRING for protein–protein interaction network construction and then imported into Cytoscape for topological analysis using the Centiscape and Network Analyzer plugins.

Molecular docking verification

SDF format ligand files for the four Danshen components were sourced from the PubChem database (<https://pubchem.ncbi.nlm.nih.gov/>, accessed on 23 July 2024). Four-dimensional structural models for the mouse proteins PIK3CG (A0A1W2P8F6), caspase-1 (CASP1, P29452), Bruton's tyrosine kinase (BTK, P35991), and Matrix metalloproteinase-9 (MMP9, P41245) were sourced from the UniProt database (<https://www.uniprot.org/>, accessed on 23 July 2024). Molecular docking analysis using ZDOCK was performed to assess the interactions between Danshen components and their target proteins. The ZDOCK module results identified docking sites and computed ZDOCK scores.

Quantitative real-time RT-PCR

Total RNA isolated from the VPL/VPM was treated with DNase I (New England Biolabs, Ipswich, MA, USA) and reverse-transcribed using the RevertAid First Strand cDNA Synthesis Kit (Thermo), utilizing oligo(dT) or specific RT primers. A 2 μ L cDNA template was amplified by real-time PCR using primers (Sangon Biotech, Shanghai, China) listed in Supplementary Table S2. Each sample

was analyzed in triplicate using a 20 μ L reaction mixture, which included 250 nM of both forward and reverse primers, 10 μ L of Thermo Scientific Maxima SYBR Green qPCR Master Mix (2 \times , Rox solution), and 20 ng of total cDNA. The reactions were performed using a 7500 Fast Real-Time PCR Detection System (Applied Biosystems, USA). The thermal cycling protocol consisted of an initial step at 95 $^{\circ}$ C for 3 min, followed by 40 cycles of 95 $^{\circ}$ C for 10 s, 60 $^{\circ}$ C for 30 s, and 72 $^{\circ}$ C for 30 s. The mRNA ratios were calculated using the $\Delta\Delta C_t$ method ($2^{-\Delta\Delta C_t}$). All the data were normalized to *Gapdh*, which is stable in mice after CPSP.

Western blot

Bilateral VPL/VPM tissues were collected from the mice and homogenized in ice-cold lysis buffer. After electrophoresis, the proteins were transferred onto PVDF membranes (Millipore, Darmstadt, Germany) at 250 mA. The membranes were blocked for 2 h at room temperature and then incubated overnight at 4 $^{\circ}$ C with primary antibodies against rabbit PIK3CG (1:1000, ab302958, Abcam), rabbit NLRP3 (1:1000, ab263899, Abcam), and rabbit GAPDH (1:1000, ab9485, Abcam). The membranes were then incubated with peroxidase-conjugated secondary antibodies for 2 h at room temperature. The immune complexes were detected using an enhanced chemiluminescence kit (Beyotime Biotechnology, Shanghai, China). Images were captured using a Bio-Rad ChemiDoc MP imaging system (Bio-Rad, USA). ImageJ software (version 2.9.0, National Institutes of Health, Bethesda, MD) was used to convert the images to 8-bit grayscale for further processing. The gel was calibrated using the "uncalibrated OD" function, after which the gel image was inverted. The target band was then selected, and its area was measured to obtain the area value.

Drug affinity responsive target stability (DARTS)

VPL/VPM tissues were collected from mice, and protein lysates were prepared as previously described. Danshenol B (purity 99%, HY-122963, MCE; CAS: 189308-09-6) was dissolved in 0.1% DMSO to prepare a 10 mM stock solution. For treatment, Danshenol B was added to 30 μ g of total protein lysate to a final concentration of 10 μ M, while control samples received an equal volume of 0.1% DMSO. The reaction volume was adjusted to 100 μ L and incubated at 4 $^{\circ}$ C for 30 min to allow sufficient interaction between the small molecule and target proteins. Trypsin (2.5%, Thermo Scientific, USA; CAS: 15090046) was then added at a 1:200 (enzyme: protein, w/w) ratio, and the mixture was incubated on ice for 20 min. The reaction was terminated by adding 25 μ L of 5 \times SDS-PAGE loading buffer (Beyotime, P0015L), followed by heating at 95 $^{\circ}$ C for 5 min to denature the proteins and halt proteolysis. The denatured samples were then subjected to Western

blot analysis as previously described. Protein bands were visualized and quantified by densitometric analysis using ImageJ software.

Statistical analysis

To minimize bias, all behavioral assessments (including the von Frey test, thermal hyperalgesia test, cold plate assay, and mNSS scoring) were performed by investigators blinded to the treatment groups. For molecular experiments, including RNA extraction, RT-qPCR, and Western blot analysis, tissue samples were assigned coded identifiers, and data acquisition and analysis were conducted in a blinded manner. Mice that died during or after the collagenase IV injection procedure were excluded from the study. In addition, for behavioral and molecular analyses, data points deviating more than two standard deviations from the group mean were considered outliers and excluded from the final analysis.

Data were randomly collected and presented as the mean \pm SD using GraphPad Prism 9. The normality of distribution for each dataset was assessed before analysis using the same software. Normality was tested using the D'Agostino–Pearson omnibus, Anderson–Darling, Shapiro–Wilk, and Kolmogorov–Smirnov tests with the Dallal–Wilkinson–Lillie for *P* value. Statistical analyses included two-tailed, unpaired Student's *t*-tests and one-way and two-way ANOVAs with repeated measures. Significant results from ANOVAs were further analyzed using post hoc Tukey tests. *P*-values less than 0.05 were considered significant.

Table 1 The mNSS of mice in the saline and coll groups on the first day post-injection

	Mean	S.D.	Min.	Max.	<i>P</i>
Motor tests					
Saline	0.1765	0.3930	0	1	0.6406
Coll	0.1176	0.3321	0	1	
Sensory tests					
Saline	0	0	0	0	
Coll	0	0	0	0	
Beam balance tests					
Saline	0.4118	0.6183	0	2	0.6537
Coll	0.5294	0.8745	0	3	
Reflex absence and abnormal movements					
Saline	0.1176	0.3321	0	1	0.6406
Coll	0.1765	0.3930	0	1	

Note: Motor tests, Unpaired *t*-test, $t=0.4714$, $df=32$; Sensory tests, Unpaired *t*-test; Beam balance tests, Unpaired *t*-test, $t=0.4529$, $df=32$; Reflex absence and abnormal movements, Unpaired *t*-test, $t=0.4714$, $df=32$. Each group consisted of 17 mice

Results

Injection of collagenase IV into the VPL/VPM led to nociceptive hypersensitivities

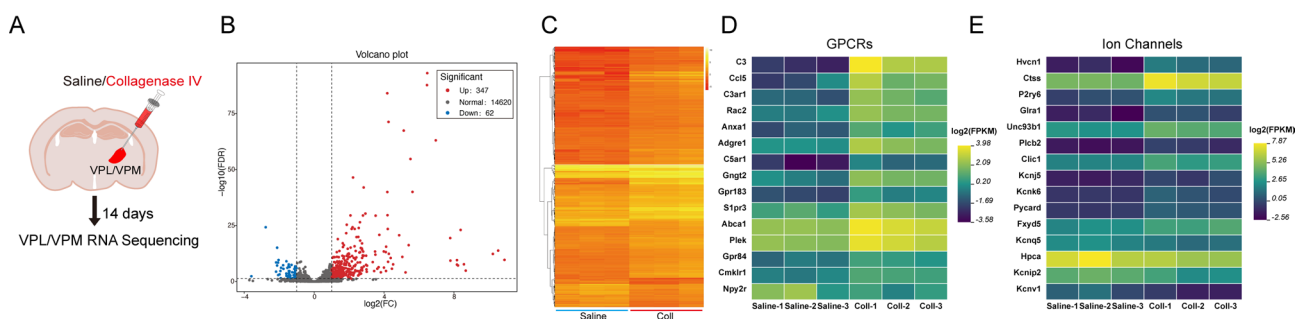
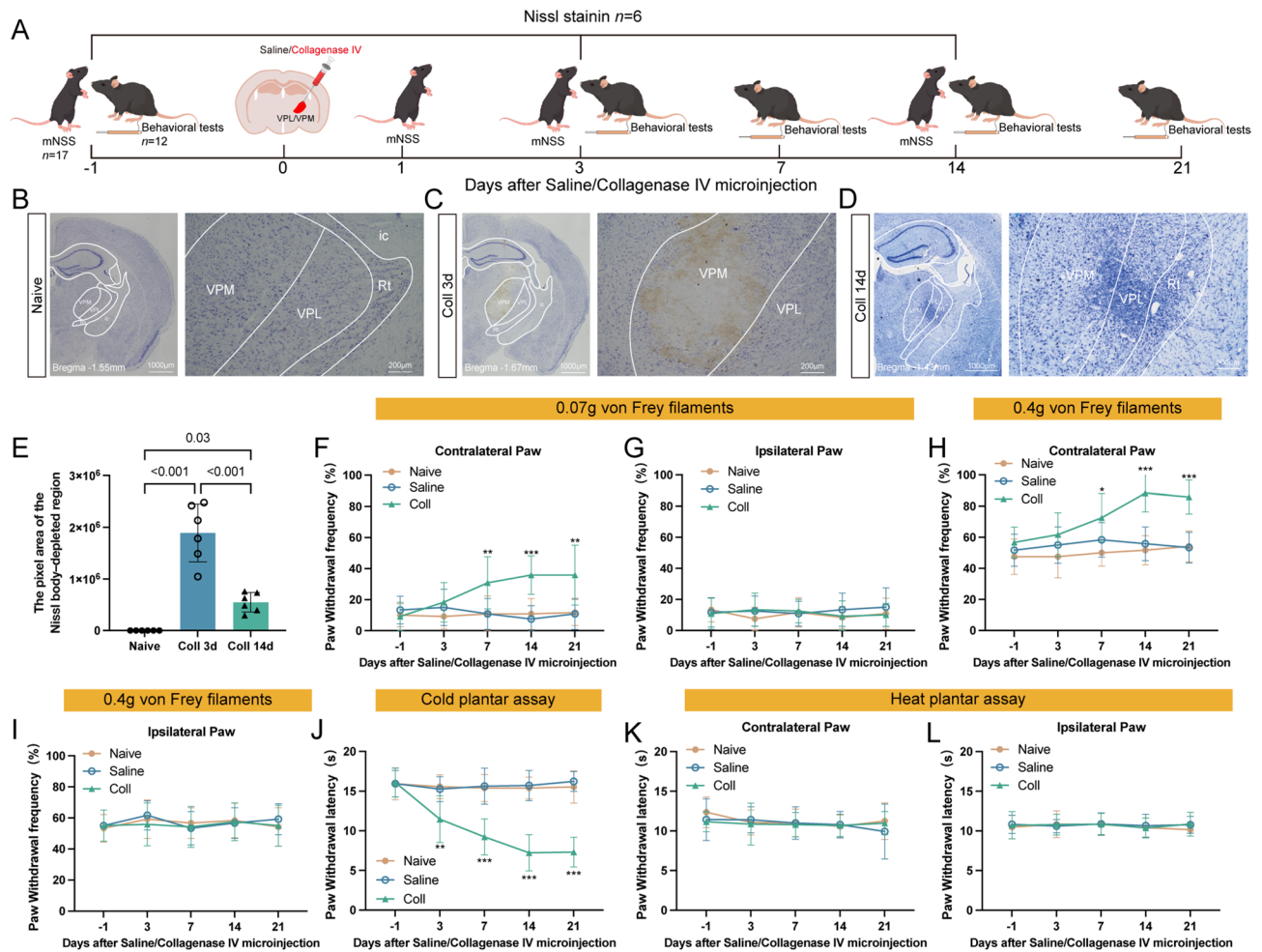
A central post-stroke pain model was created by injecting collagenase IV (0.01 U/10 nL) into the right VPL/VPM junction in mice (Coll group). The control group received saline (10nL) injections (Saline group). The mNSS was evaluated in both groups 1 day before injection and at 1, 3, and 14 days post-injection. No significant differences were observed between the two groups, indicating that normal motor function, balance, and reflexes remained intact (Supplementary Fig. 2, Table 1). Nissl bodies in the VPL/VPM region were examined 3 (Coll 3d group) and 14 (Coll 14d group) days postinjection. Compared with the Naive group, the Coll 3d and Coll 14d groups exhibited significant loss of Nissl bodies in the right VPL/VPM ($P=0.03$, $P<0.001$; Figs. 1A–E). We repeated the Saline and collagenase IV injections and evaluated pain behavior in the mice. In the Coll group, mechanical allodynia in the contralateral hind paw emerged on day 7 postinjection ($*P<0.05$, $**P<0.01$; Figs. 1E, H), while no abnormalities were observed in the ipsilateral hind paw compared to the Naive group (Figs. 1G, I). Cold hyperalgesia was similarly observed in the Coll group ($**P<0.01$, $***P<0.001$; Fig. 1J). However, neither the Saline nor the Coll group exhibited heat hyperalgesia compared to the Naive group (Figs. 1K, L). These results confirm the successful establishment of a CPSP model in mice.

Altered expression profiles of mRNAs in the VPL/VPM after CPSP

We repeated the saline and collagenase IV injections and collected VPL/VPM tissue from the Saline and Coll group mice for transcriptomic sequencing on the 14th day post-injection (Fig. 2A). Significant changes in mRNA expression within the VPL/VPM were observed after CPSP. Specifically, about 409 DEGs (347 upregulated, 62 downregulated) presented substantial changes in expression levels (Fig. 2B). Clustered heatmaps of DEGs revealed distinct gene expression patterns in the VPL/VPM after CPSP (Fig. 2C). G protein-coupled receptors (GPCRs) and ion channels are crucial for transmitting and modulating nociceptive information. Among the DEGs, 133 were identified as GPCR mRNAs, and 226 were identified as ion channel mRNAs in the VPL/VPM. The heatmaps display the top 15 upregulated and downregulated DEGs for both GPCRs (Fig. 2D) and ion channels (Fig. 2E) in the VPL/VPM.

Functional enrichment analysis of the DEGs after CPSP

To analyze the functional enrichment of these DEGs, we used clusterProfiler for GO, KEGG and euKaryotic Ortholog Groups (KOG) pathway analyses to categorize the upregulated and downregulated DEGs by distinct



processes. We screened the transcriptomic data for CPSP-related pathways and found that the upregulated DEGs were predominantly enriched in inflammation-associated pathways according to GO analysis (Fig. 3A). In contrast, the downregulated DEGs were mainly associated with oxidative stress-related pathways (Fig. 3B). KEGG analysis further revealed that the upregulated DEGs were primarily enriched in pathways related to inflammation and apoptosis (Fig. 3C). Notably, no CPSP-relevant pathways were enriched among the downregulated DEGs in the KEGG analysis.

Enrichment analyses of KOG, GO, and KEGG pathways revealed distinct functional distributions of the DEGs. Specifically, KOG enrichment analysis showed that 48 upregulated DEGs were associated with signal transduction pathways, while 26 upregulated DEGs were related to cytoskeletal organization and extracellular structure (Supplementary Fig. 3A, Supplementary Table S3). In contrast, the 62 downregulated DEGs were dispersed across multiple functional categories without significant enrichment in any single category (Supplementary Fig. 3B, Supplementary Table S4). GO enrichment analysis revealed that the upregulated DEGs were enriched in immune system processes, biological adhesion, and cell killing within the biological process category (Supplementary Fig. 3C, Supplementary Table S5). For molecular function, they were enriched in electron carrier activity and chemoattractant activity (Supplementary Fig. 3C, Supplementary Table S5). Downregulated DEGs were mainly linked to biological adhesion, rhythmic processes, and synapse part functions (Supplementary Fig. 3D, Supplementary Table S6). In the network diagram of DEGs and GO pathways, the top five pathways with the smallest *P*-values were chosen for analysis. The analysis revealed

upregulated DEGs such as *Cst7*, *newGene_6227*, *Cd5l*, *Clec7a*, *Mmp12*, and *Saa3* (Supplementary Figs. 4A, C, E), and downregulated DEGs including *Gbp3*, *Ifi203*, *Irgm2*, *Oasl2*, *Gbp9*, *Cplx3*, *Kcnq5*, and *Trh* (Supplementary Figs. 4A, B, D, F), all of which showed significant changes. The pathways associated with each gene are listed in Supplementary Table S7. To systematically identify the lineage programs altered during CPSP and avoid missing genes that may have biological significance despite not being significantly differentially expressed, we performed GSEA. GO pathways were used as the gene sets of interest, and the top five gene sets with the lowest *P*-values were identified. Functions such as signal transduction, response to stimuli (Supplementary Figs. 5A, C), the extracellular region (Supplementary Fig. 5B), and metalloendopeptidase activity (Supplementary Fig. 5C) were found to play important roles in CPSP. The results of the GO enrichment analysis were visualized using directed acyclic graphs, with branches illustrating inclusion relationships from broader to narrower categories. The top 10 GO enrichments functioned as master nodes. These were presented alongside related GO terms and systematically organized categories. Directed acyclic graphs were created for biological processes, molecular functions, and cellular components within the VPL/VPM (Supplementary Fig. 6).

KEGG pathway analysis showed that the upregulated DEGs were enriched mainly in the phagosome and tuberculosis pathways (Supplementary Fig. 3E, Supplementary Table S8), while the downregulated DEGs were enriched in hepatitis C and the NOD-like receptor signaling pathway (Supplementary Fig. 3E, Supplementary Table S9). The top five pathways with the lowest *P*-values were chosen for analysis in the network diagram of DEGs and

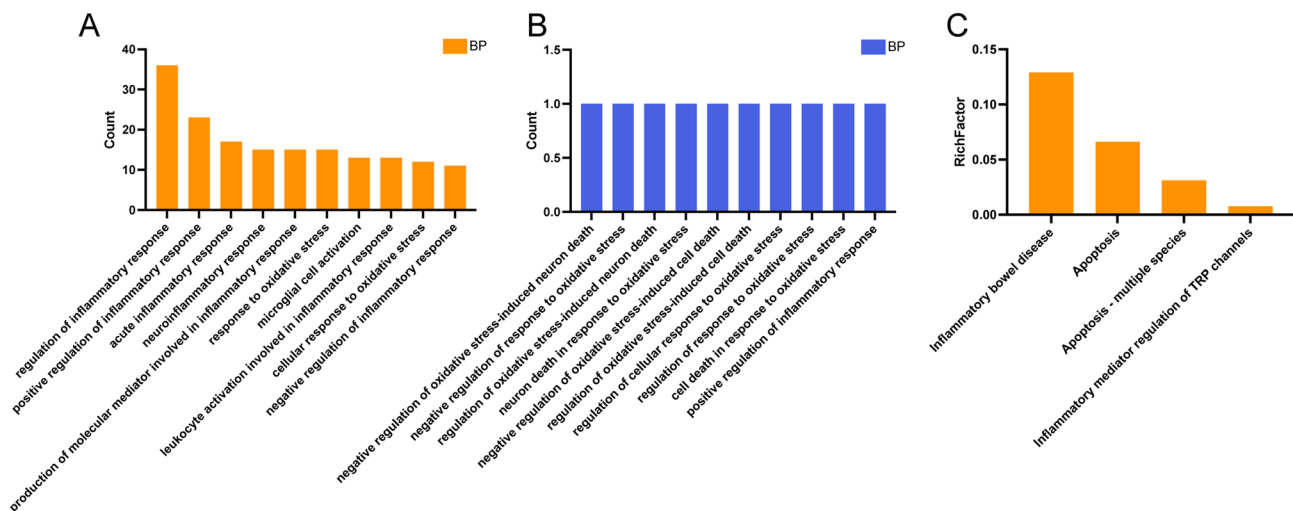


Fig. 3 Analysis results of CPSP-related pathways in GO and KEGG analyses. **(A):** Perform GO analysis on the upregulated DEGs after CPSP modeling, and screen for CPSP-related pathways, listing the top 10. **(B):** Perform GO analysis on the downregulated DEGs after CPSP modeling, and screen for CPSP-related pathways, listing the top 10. **(C):** Perform KEGG analysis on the upregulated DEGs after CPSP modeling, and screen for CPSP-related pathways

KEGG pathways. The study revealed that upregulated DEGs such as *Atp6v0d2*, *Clec7a*, and *Itgax* (Supplementary Fig. 4G) and downregulated DEGs such as *Irgm2*, *Gbp3*, and *Oasl2* (Supplementary Fig. 4H) exhibited significant changes. The pathways related to each gene are listed in Supplementary Table S10. Similarly, GSEA was performed using KEGG pathways as the gene sets of interest, and the top five gene sets with the lowest *P* values were identified. Pathways related to cancer, viral infection, and the PI3K-Akt signaling pathway were found to exhibit significant changes in CPSP (Supplementary Fig. 7).

To understand the functional interactions among DEGs and their potential involvement in neuropathic pain, a PPI network was constructed using the STRING database (<https://string-db.org/>). The network was constructed using the top 50 protein-coding DEGs with the strongest correlations in the VPL/VPM. As illustrated in Supplementary Fig. 8, the upregulated DEGs, including *Ptprc*, *Itgam*, *Fcgr3*, *Cd44*, and *Cd86* are crucial molecules among the hub genes in the VPL/VPM network (Supplementary Table S11).

Screening potential therapeutic targets for CPSP using components of Danshen

Among the 42 identified components of Danshen (Supplementary Table S12), 235 targets were predicted using the Swiss Target Prediction database (Supplementary Table S13). A network in which Danshen components were mapped to their targets was constructed with Cytoscape 3.9.1 (Fig. 4A). Notably, tanshinaldehyde and (6*S*)-6-(hydroxymethyl)-1,6-dimethyl-8,9-dihydro-7*H*-naphtho[8,7-*g*]benzofuran-10,11-dione (Mol name: MOL007155) exhibited the highest number of associated potential targets at 100 each, followed by Danshenol B (94), Danshenol A (73), luteolin (58), and sclareol (48). The study identified 409 DEGs in the ipsilateral VPL/VPM of CPSP model mice. After excluding 11 novel genes, 398 DEGs remained. A Venn diagram was created to show overlaps between the predicted targets of Danshen and the DEGs in CPSP. The analysis revealed 11 potential candidate targets for treating CPSP with Danshen (Fig. 4B).

The PPI network for the 11 intersecting targets was created using the STRING database and visualized using Cytoscape 3.9.1 (Fig. 4C). The network consisted of 11 nodes and 76 edges, with node size and color representing their degree values. *Btk*, *Mmp9*, *Casp1*, *Ctss*, *Ccr5*, and *Pik3cg* presented the highest degree values among the targets, at 10, 9, 9, 8, 8, and 8, respectively (Supplementary Table S14). Topological analysis revealed that *Btk* had the highest betweenness centrality score of 0.1589, followed by *Pik3cg* at 0.070 and *Mmp9* and *Casp1* at 0.048, suggesting that *Btk* is the most crucial

component within this network (Supplementary Table S14).

To comprehensively understand how Danshen components affect CPSP at the system level, KEGG and GO enrichment analyses were performed on the 11 intersecting targets. In the KEGG enrichment analysis, the top 15 pathways with the lowest *P*-values ($P < 0.05$) were selected, including primary immunodeficiency ($P < 0.001$), the chemokine signaling pathway ($P < 0.01$), NF- κ B signaling pathway ($P < 0.01$), and toxoplasmosis ($P < 0.01$) (Fig. 4D, Supplementary Table S15). Additionally, GO enrichment analysis revealed that the targets were involved in 742 biological processes, 45 cellular components, and 80 molecular functions (Supplementary Table S16). As shown in Fig. 4E, the main enriched terms in the BP category included regulation of the inflammatory response ($P < 0.001$), positive regulation of the inflammatory response ($P < 0.001$), and myeloid leukocyte activation ($P < 0.001$). The CC category was significantly enriched in the extrinsic component of the membrane and the cytoplasmic side of the plasma membrane, both with notable results ($P < 0.001$). In the MF category, significant enrichment was observed for nonmembrane-spanning protein tyrosine kinase activity ($P < 0.001$).

Molecular docking between danshen components and therapeutic targets

To identify the key Danshen components for CPSP, an interaction network involving 21 Danshen components and 11 intersecting targets was constructed (Fig. 4F). The remaining 21 Danshen components do not target these 11 genes. Among the 21 Danshen components, MOL007155 exhibited the highest degree value at 8, followed by tanshinaldehyde and Danshenol B at 6, and sclareol at 4 (Supplementary Table S17). Topological analysis revealed that MOL007155 had the highest betweenness centrality score of 494.43, followed by tanshinaldehyde at 303.51, Danshenol B at 286.89, and sclareol at 100.09 (Supplementary Table S17). In conclusion, MOL007155, tanshinaldehyde, Danshenol B, and sclareol are likely the crucial Danshen components for combating CPSP.

Molecular docking was used to assess the binding affinities between four Danshen components—MOL007155, tanshinaldehyde, Danshenol B, and sclareol—and the key target proteins BTK, CASP1, MMP9, and PIK3CG (Fig. 5). The docking scores ranged from -7.111 to -9.619 kcal/mol, all below -7.000 kcal/mol, indicating strong binding affinities [39]. The binding pockets of BTK, CASP1, MMP9, and PIK3CG are tightly occupied by these components and are stabilized through hydrogen bonds and hydrophobic interactions (Supplementary Table S18). This finding indicates the effective binding of Danshen components to core targets via hydrogen

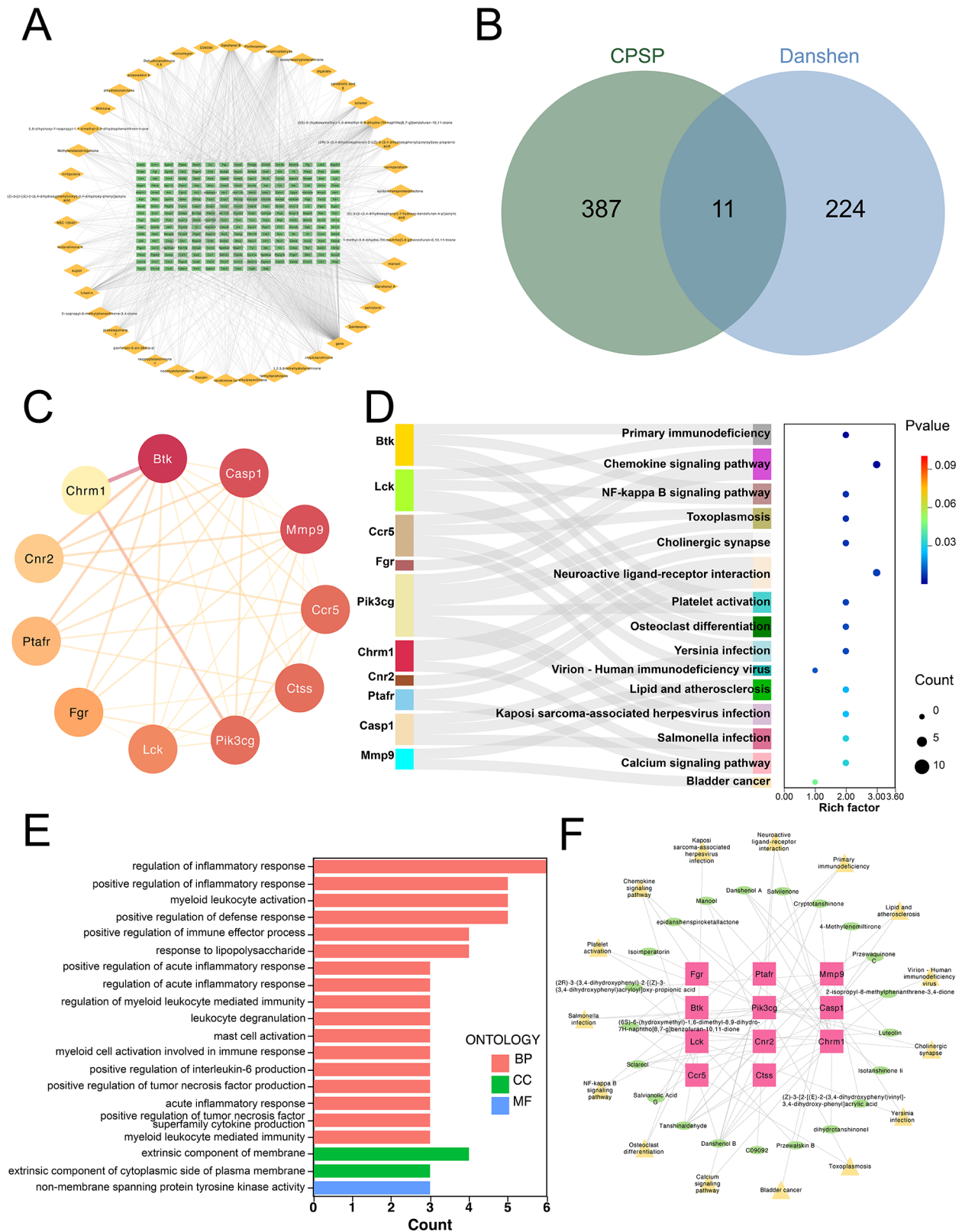


Fig. 4 Transcriptomic intervention analysis of Danshen components in a mouse model of CPSP. **(A):** Construction of the Danshen–targets network. **(B):** Venn diagram of predicted Danshen targets and DEGs. **(C):** PPI network of interesting 11 targets. **(D):** KEGG pathway analysis of 11 key targets. **(E):** GO enrichment analysis of 11 key targets. **(F):** Danshen-targets-CPSP network diagram

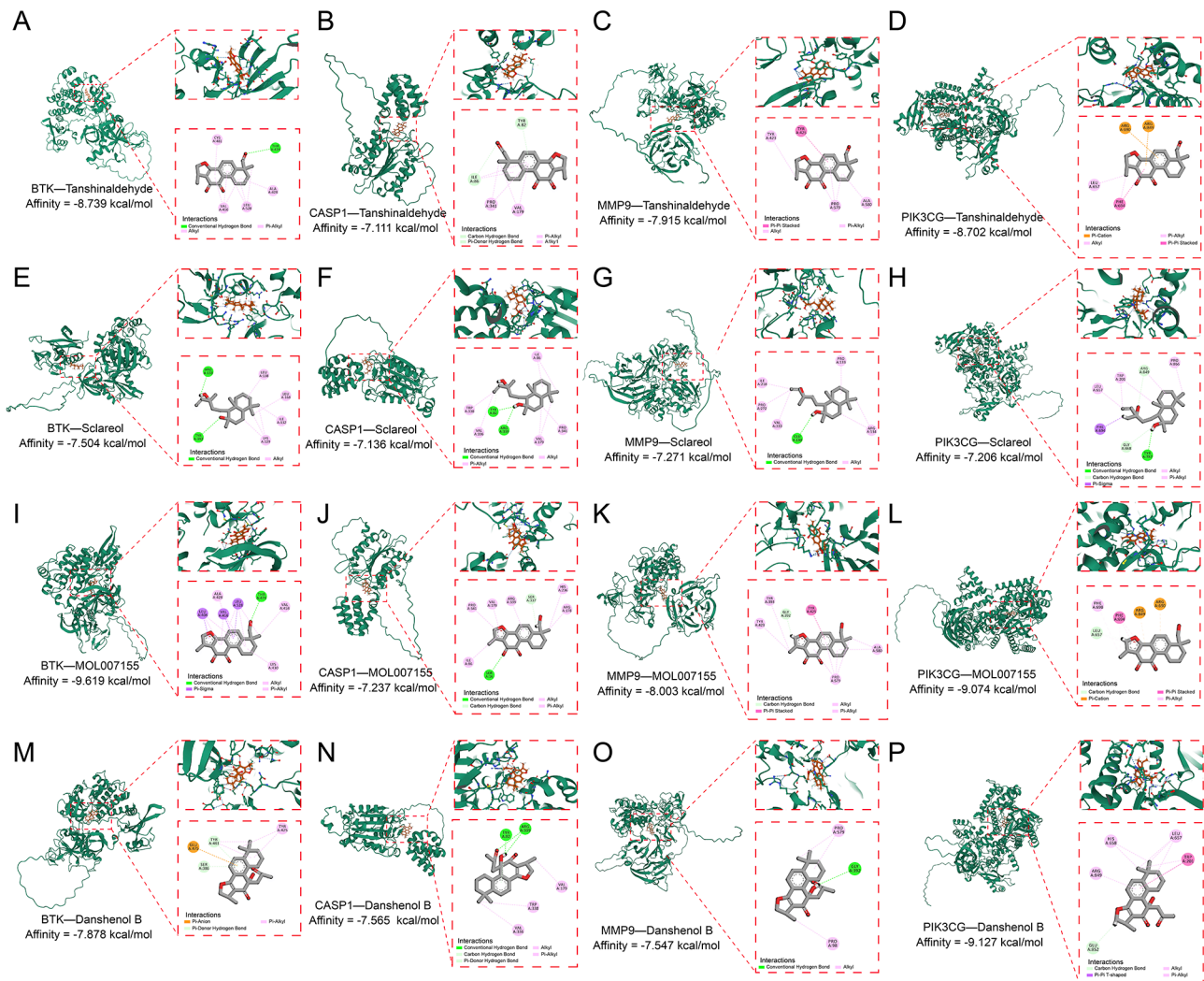


Fig. 5 Molecular docking of main Danshen components with BTK, CASP1, MMP9, PIK3CG. **(A):** Interaction diagram between BTK and Tanshinaldehyde. **(B):** Interaction diagram between CASP1 and Tanshinaldehyde. **(C):** Interaction diagram between MMP9 and Tanshinaldehyde. **(D):** Interaction diagram between PIK3CG and Tanshinaldehyde. **(E):** Interaction diagram between BTK and Scclareol. **(F):** Interaction diagram between CASP1 and Scclareol. **(G):** Interaction diagram between MMP9 and Scclareol. **(H):** Interaction diagram between PIK3CG and Scclareol. **(I):** Interaction diagram between BTK and MOL007155. **(J):** Interaction diagram between CASP1 and MOL007155. **(K):** Interaction diagram between MMP9 and MOL007155. **(L):** Interaction diagram between PIK3CG and MOL007155. **(M):** Interaction diagram between BTK and Danshenol B. **(N):** Interaction diagram between CASP1 and Danshenol B. **(O):** Interaction diagram between MMP9 and Danshenol B. **(P):** Interaction diagram between PIK3CG and Danshenol B

bonds and hydrophobic interactions. Notably, the strongest binding affinity was between MOL007155 and BTK (-9.619 kcal/mol), followed by Danshenol B and PIK3CG (-9.127 kcal/mol) (Fig. 5).

Administration of danshenol B effectively alleviates CPSP in mice

To confirm the consistency of transcriptomic sequencing results, we performed RT-qPCR to quantify the mRNA expression levels of *Btk*, *Casp1*, *Mmp9*, and *Pik3cg* in the ipsilateral VPL/VPM of Saline and Coll groups on days 3 and 14 after modeling. On day 3, only *Mmp9* mRNA ($P=0.007$) expression was significantly elevated in the Coll 3d group. By day 14, the mRNA levels of *Btk*

($P=0.0154$), *Casp1* ($P=0.0140$), *Mmp9* ($P=0.0190$), and *Pik3cg* ($P=0.0174$) were significantly increased in the Coll group compared to the Saline group (Figs. 6A–E). Given the challenges in acquiring MOL007155 and the high expression of PI3K pathway genes in the CPSP model, as shown in Supplementary Fig. 7A, we focused on the interaction between PIK3CG and Danshenol B to investigate its role in treating CPSP. A DARTS assay using VPL/VPM tissue from naïve mice demonstrated that Danshenol B binds to PIK3CG and enhances its resistance to proteolytic degradation, further confirming the direct interaction between Danshenol B and the PIK3CG protein ($P=0.0171$, Supplementary Fig. 9). By day 14 post-surgery, PIK3CG protein was significantly higher

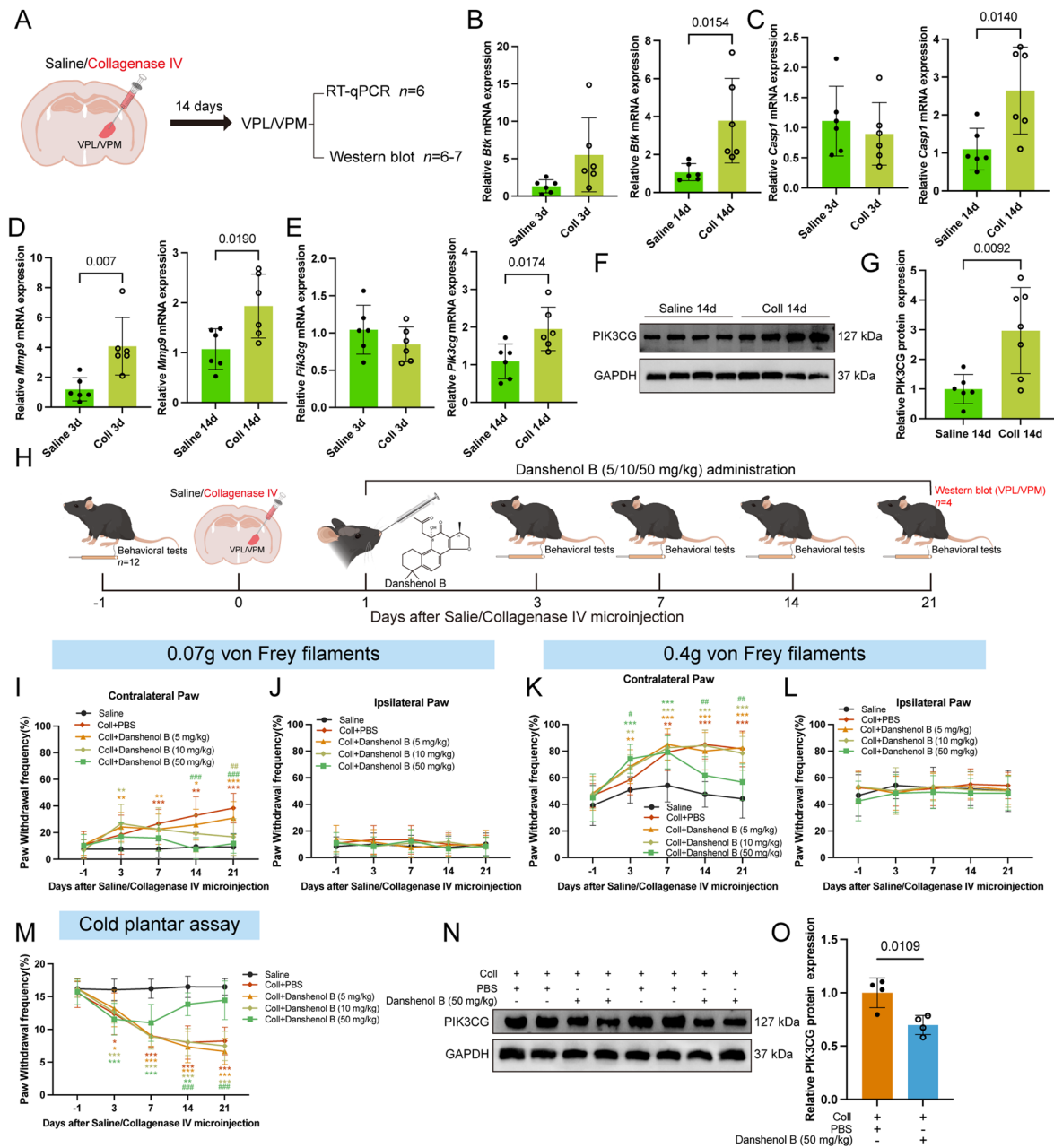


Fig. 6 Danshenol B can alleviate mechanical allodynia and cold hyperalgesia in CPSP. **(A)**: Saline or collagenase IV was injected into the VPL/VPM of mice, and the mRNA and protein expression in the ipsilateral VPL/VPM were evaluated 14 days post-injection. **(B–E)**: The mRNA levels of *Btk* **(B)**, *Casp1* **(C)**, *Mmp9* **(D)**, and *Pik3cg* **(E)** (unpaired *t*-test, $t = 2.054$, $df = 10$. $P = 0.07$, $n = 6$ in B left; unpaired *t*-test, $t = 2.915$, $df = 10$. $P = 0.0154$, $n = 6$ in B right; unpaired *t*-test, $t = 0.6782$, $df = 10$. $P = 0.51$, $n = 6$ in C left; unpaired *t*-test, $t = 2.973$, $df = 10$. $P = 0.0140$, $n = 6$ in C right; unpaired *t*-test, $t = 3.4$, $df = 10$. $P = 0.007$, $n = 6$ in D left; unpaired *t*-test, $t = 2.794$, $df = 10$. $P = 0.0190$, $n = 6$ in D right; unpaired *t*-test, $t = 1.198$, $df = 10$. $P = 0.26$, $n = 6$ in E left; unpaired *t*-test, $t = 2.846$, $df = 10$. $P = 0.0174$, $n = 6$ in E right). **(F–G)**: Fourteen days post-injection, PIK3CG protein in the ipsilateral VPL/VPM of the Coll group was higher compared to the Saline group (unpaired *t*-test, $t = 3.152$, $df = 11$; $P = 0.0092$, $n = 6$ in Saline group, $n = 7$ in Coll group). **(H)**: Timeline of drug administrations and pain behavior assessment time points. **(I–J)**: PWF for contralateral **(I)** and ipsilateral **(J)** hind paws in each group, tested using 0.07 g von Frey filaments **(I)**: two-way ANOVA followed by Tukey's test, $F_{(16, 220)} = 3.587$, $P < 0.001$. **J**: two-way ANOVA followed by Tukey's test, $F_{(16, 220)} = 0.6591$, $P = 0.83$; * $P < 0.05$, ** $P < 0.01$, *** $P < 0.001$ vs. Saline group; ## $P < 0.01$, ### $P < 0.001$ vs. Coll + PBS group; $n = 12$). **(K–L)**: PWF for contralateral **(K)** and ipsilateral **(L)** hind paws in each group, tested using 0.4 g von Frey filaments **(K)**: two-way ANOVA followed by Tukey's test, $F_{(16, 220)} = 5.003$, $P < 0.001$. **L**: two-way ANOVA followed by Tukey's test, $F_{(16, 220)} = 0.4380$, $P = 0.97$; * $P < 0.05$, ** $P < 0.01$ vs. Saline group; # $P < 0.05$, ## $P < 0.01$ vs. Coll + PBS group; $n = 12$). **(M)**: PWL for each group of mice, measured using a 0 °C cold plate (two-way ANOVA followed by Tukey's test, $F_{(16, 220)} = 12.15$, $P < 0.001$; * $P < 0.05$, *** $P < 0.001$ vs. Saline group; ### $P < 0.001$ vs. Coll + PBS group; $n = 12$). **(N–O)**: 21 days post-injection, PIK3CG protein in the ipsilateral VPL/VPM of mice was lower in the Coll + Danshenol B group compared to the Coll + PBS group (unpaired *t*-test, $t = 3.633$, $df = 6$; $P = 0.0109$, $n = 4$).

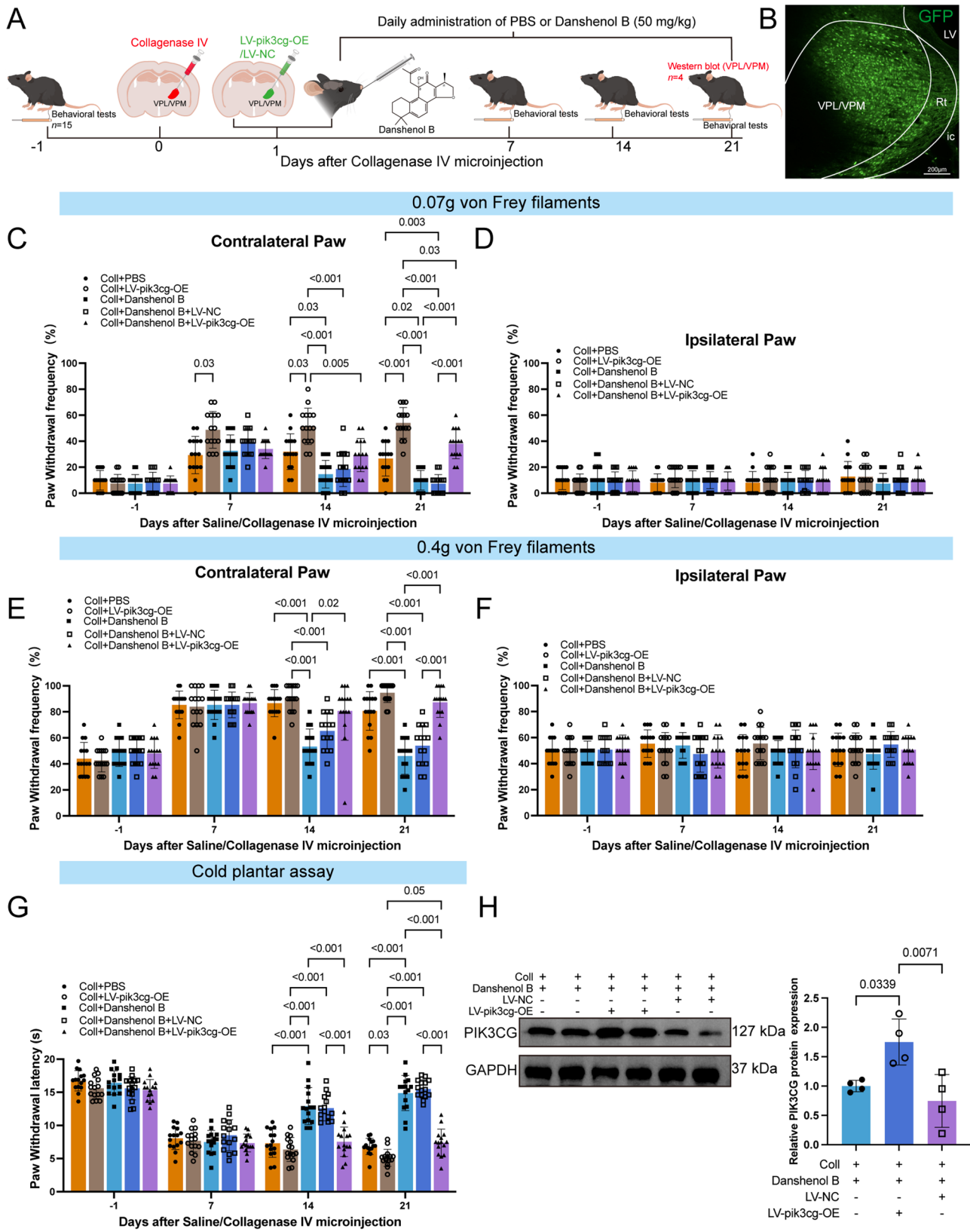


Fig. 7 (See legend on next page.)

(See figure on previous page.)

Fig. 7 Danshenol B alleviates CPSP by regulating PIK3CG protein. **(A)**: Collagenase IV was injected into the VPL/VPM of mice, and one day later, either the PIK3CG overexpression virus (LV-pik3cg-OE) or the control virus (LV-NC) was injected into the VPL/VPM of the two groups of mice. Meanwhile, mice were administered Danshenol B (50 mg/kg) or PBS daily via oral gavage. Pain behaviors were assessed, and on day 21, PIK3CG protein levels in the ipsilateral VPL/VPM were measured. **(B)**: Observation of lentiviral-mediated GFP gene expression in VPL/VPM brain tissue using a fluorescence microscope. scale bar = 200 μ m. **(C–D)**: PWF for contralateral **(C)** and ipsilateral **(D)** hind paws in each group, tested using 0.07 g von Frey filaments (C: two-way ANOVA followed by Sidak test, $F_{(12, 210)} = 14.31$, $P < 0.001$. D: two-way ANOVA followed by Sidak test, $F_{(12, 210)} = 0.6969$, $P = 0.75$; $n = 15$). **(E–F)**: PWF for contralateral **(E)** and ipsilateral **(F)** hind paws in each group, tested using 0.4 g von Frey filaments (E: two-way ANOVA followed by Sidak test, $F_{(12, 210)} = 13.48$, $P < 0.001$. F: two-way ANOVA followed by Sidak test, $F_{(12, 210)} = 0.9567$, $P = 0.49$; $n = 15$). **(G)**: PWL for each group of mice, measured using a 0 °C cold plate (two-way ANOVA followed by Sidak test, $F_{(12, 210)} = 27.49$, $P < 0.001$; $n = 15$). **(H)**: 21 days post-injection, PIK3CG protein increased in the Coll + Danshenol B + LV-pik3cg-OE group relative to the Coll + Danshenol B + LV-NC group (one-way ANOVA, $F_{(2, 9)} = 8.958$, $P = 0.0072$; $n = 4$)

in the ipsilateral VPL/VPM of the Coll 14d group than in controls ($P = 0.0092$, Figs. 6F–G). To investigate the regulatory effects of Danshenol B on PIK3CG and CPSP, we orally administered varying concentrations (5/10/50 mg/kg) of Danshenol B to mice (Coll + Danshenol B group) once daily for 21 consecutive days, while the control group received PBS (Coll + PBS group). We assessed PIK3CG protein expression in the ipsilateral VPL/VPM and evaluated pain-related behaviors in mice (Fig. 6H). Continuous administration of Danshenol B (50 mg/kg) for 14 days alleviated Coll-induced mechanical allodynia ($##P < 0.01$, $###P < 0.001$, Figs. 6I, K) and cold hyperalgesia ($###P < 0.001$, Fig. 6M) in the contralateral hind paw, without altering the ipsilateral hind paw's pain threshold (Fig. 6J, L). Lower doses of 5 mg/kg and 10 mg/kg did not alleviate pain (Figs. 6I–M). After completing the behavioral test (at 21 days post-injection), ipsilateral VPL/VPM tissues were collected from mice in the Coll + PBS group and the Coll + Danshenol B (50 mg/kg) group for Western blot analysis and RT-qPCR. The PIK3CG protein level in the ipsilateral VPL/VPM was significantly lower in the Coll + Danshenol B group compared to the Coll + PBS group ($P = 0.0109$, Figs. 6N–O). However, no significant changes were observed in the mRNA levels of *Btk*, *Casp1*, *Mmp9*, and *Pik3cg* (Supplementary Fig. 10). These results suggest that continuous administration of Danshenol B (50 mg/kg) reduces PIK3CG and alleviates mechanical allodynia and cold hyperalgesia.

Danshenol B alleviates pain by inhibiting the PIK3CG/NLRP3 signaling pathway

To investigate the role of PIK3CG in Danshenol B's pain-relieving effects, we administered 50 mg/kg of Danshenol B (Coll + Danshenol B group) or PBS (Coll + PBS group) daily, starting one day after CPSP model establishment, alongside lentiviral overexpression of PIK3CG (Coll + Danshenol B + LV-pik3cg-OE group). The control group received a negative control virus (Coll + Danshenol B + LV-NC group) (Fig. 7A). Twenty-one days after collagenase IV injection, green fluorescent protein (GFP)-positive neurons, infected by the virus, were predominantly observed in the VPL/VPM (Fig. 7B). After 21 days, the Coll + Danshenol B + LV-pik3cg-OE group showed increased mechanical and cold pain sensitivity in

the contralateral hind paw compared to the Coll + Danshenol B + LV-NC group ($P < 0.001$, Figs. 7C, E, G). No differences were observed in PWF of the ipsilateral hind paw among the groups (Figs. 7D, F). After completing the behavioral assessments on day 21, ipsilateral VPL/VPM tissues from the Coll + Danshenol B group, Coll + Danshenol B + LV-NC group, and Coll + Danshenol B + LV-pik3cg-OE group were collected for Western blot analysis. Western blot revealed elevated PIK3CG protein in the ipsilateral VPL/VPM of the Coll + Danshenol B + LV-pik3cg-OE group, relative to the Coll + Danshenol B ($P = 0.0339$) and Coll + Danshenol B + LV-NC ($P = 0.0071$) groups (Fig. 7H).

To investigate PIK3CG's regulatory effects on pain, we administered lentiviral shRNA to knockdown PIK3CG in the ipsilateral VPL/VPM (Coll + sh-pik3cg group), post-CPSP model establishment, with controls receiving a control virus (Coll + sh-NC group) (Fig. 8A). By day 14 post-injection, the PWF to 0.07 g von Frey filament stimulation in the contralateral hind paw was lower in the Coll + sh-pik3cg group than in the controls ($P = 0.04$, Fig. 8B). On days 14 and 21, the PWF to 0.4 g von Frey filament stimulation in the contralateral hind paw was reduced in the Coll + sh-pik3cg group compared to the Coll + sh-NC group ($P < 0.001$, Fig. 8D). sh-pik3cg injection did not alter the PWF in the ipsilateral hind paw (Fig. 8C, E) but increased the PWL ($P < 0.001$, Fig. 8F). After completing pain behavior assessments on day 21, ipsilateral VPL/VPM tissues from the two groups of mice were collected for immunofluorescence staining, RT-qPCR, and Western blot analysis. GFP expression was primarily observed in the VPL/VPM, confirming successful viral infection in the targeted area (Fig. 8G). shRNA injection effectively decreased *Pik3cg* mRNA ($P = 0.0247$, Fig. 8H) and protein ($P = 0.0004$, Fig. 8I) levels in the VPL/VPM.

Research indicates that PIK3CG activation of NLRP3 contributes to septic myocardial injury [40]. To investigate whether a similar regulatory relationship exists in CPSP, we examined NLRP3 protein expression following PIK3CG modulation in the CPSP model. NLRP3 protein was significantly elevated in the ipsilateral VPL/VPM of the Coll group compared to controls ($P = 0.0136$, Fig. 8J). Danshenol B treatment decreased NLRP3 compared to

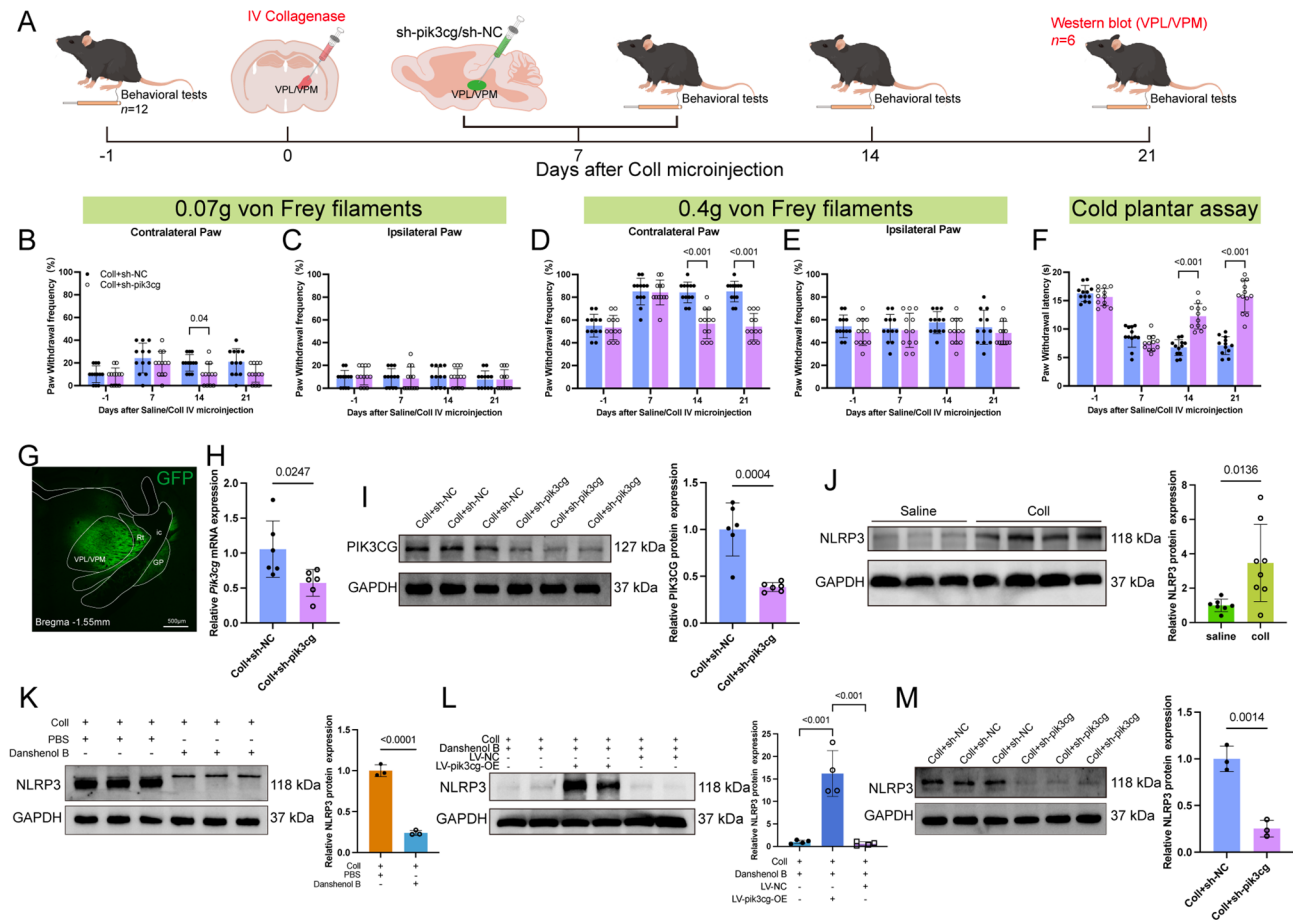


Fig. 8 Danshenol B alleviates CPSP by inhibiting the PIK3CG/NLRP3 signaling pathway. **(A)**: Timeline schematic for CPSP model establishment, virus injection, and pain behavior testing time points. **(B–C)**: PWF for contralateral **(B)** and ipsilateral **(C)** hind paws in each group, tested using 0.07 g von Frey filaments **(B)**: two-way ANOVA followed by Sidak test, $F_{(3,66)} = 1.021$, $P = 0.39$. **(C)**: two-way ANOVA followed by Sidak test, $F_{(3,66)} = 0.2457$, $P = 0.86$; $n = 12$. **(D–E)**: PWF for contralateral **(D)** and ipsilateral **(E)** hind paws in each group, tested using 0.4 g von Frey filaments **(D)**: two-way ANOVA followed by Sidak test, $F_{(3,66)} = 13.47$, $P < 0.001$. **(E)**: two-way ANOVA followed by Sidak test, $F_{(3,66)} = 0.2635$, $P = 0.85$; $n = 12$. **(F)**: PWL for each group of mice, measured using a 0 °C cold plate (two-way ANOVA followed by Sidak test, $F_{(3,66)} = 38.81$, $P < 0.001$; $n = 12$). **(G)**: Observation of lentiviral-mediated GFP gene expression in VPL/VPM brain tissue using a fluorescence microscope. scale bar = 500 μm . **(H)**: 21 days post-injection, *Pik3cg* mRNA decreased in the Coll + sh-pik3cg group relative to the Coll + sh-NC group (unpaired *t*-test, $t = 2.641$, $df = 10$; $n = 6$). **(I)**: 21 days post-injection, PIK3CG protein decreased in the Coll + sh-pik3cg group relative to the Coll + sh-NC group (unpaired *t*-test, $t = 5.252$, $df = 10$; $n = 6$). **(J)**: 14 days post-injection, NLRP3 protein increased in the Coll group relative to the Saline group (unpaired *t*-test, $t = 2.853$, $df = 13$; $n = 7$ in Saline group, $n = 8$ in Coll group). **(K)**: 21 days post-injection, NLRP3 protein decreased in the Coll + Danshenol B group relative to the Coll + P group (unpaired *t*-test, $t = 16.95$, $df = 4$; $n = 3$). **(L)**: 21 days post-injection, NLRP3 protein increased in the Coll + Danshenol B + LV-pik3cg-OE group relative to the Coll + Danshenol B + LV-NC group (one-way ANOVA, $F_{(2,9)} = 36.02$, $P < 0.001$; $n = 4$). **(M)**: 21 days post-injection, NLRP3 protein decreased in the Coll + sh-pik3cg group relative to the Coll + sh-NC group (unpaired *t*-test, $t = 7.932$, $df = 4$; $n = 3$)

the Coll + PBS group in the Coll + Danshenol B group ($P < 0.0001$, Fig. 8K). However, PIK3CG overexpression reversed the Danshenol B-induced reduction in NLRP3 ($P < 0.001$, Fig. 8L). Knockdown of PIK3CG in the CPSP model also reduced NLRP3 ($P = 0.0014$, Fig. 8M).

PIK3CG modulates the development of CPSP through NLRP3-mediated signaling pathways

To investigate whether the regulatory effect of PIK3CG on CPSP is mediated through NLRP3, we first established a CPSP mouse model and, seven days later, injected lentiviruses encoding PIK3CG-targeting shRNA along with an NLRP3 overexpression construct into the ipsilateral

VPL/VPM. Pain-related behaviors and NLRP3 protein expression in the VPL/VPM were subsequently assessed (Fig. 9A). Fourteen days after viral injection, the PWF of the contralateral hind paw was significantly increased in the NLRP3 overexpression group compared to the control group ($P = 0.007$ and $P < 0.001$; Figs. 9B, D), while the PWL was significantly reduced ($P < 0.001$; Fig. 9F). In contrast, no significant difference in the PWF of the ipsilateral hind paw was observed between the two groups (Figs. 9C, E). Consistently, Western blot analysis revealed a significant elevation in NLRP3 protein expression in the VPL/VPM of the NLRP3 overexpression group ($P < 0.001$; Fig. 9G–H). These findings indicate

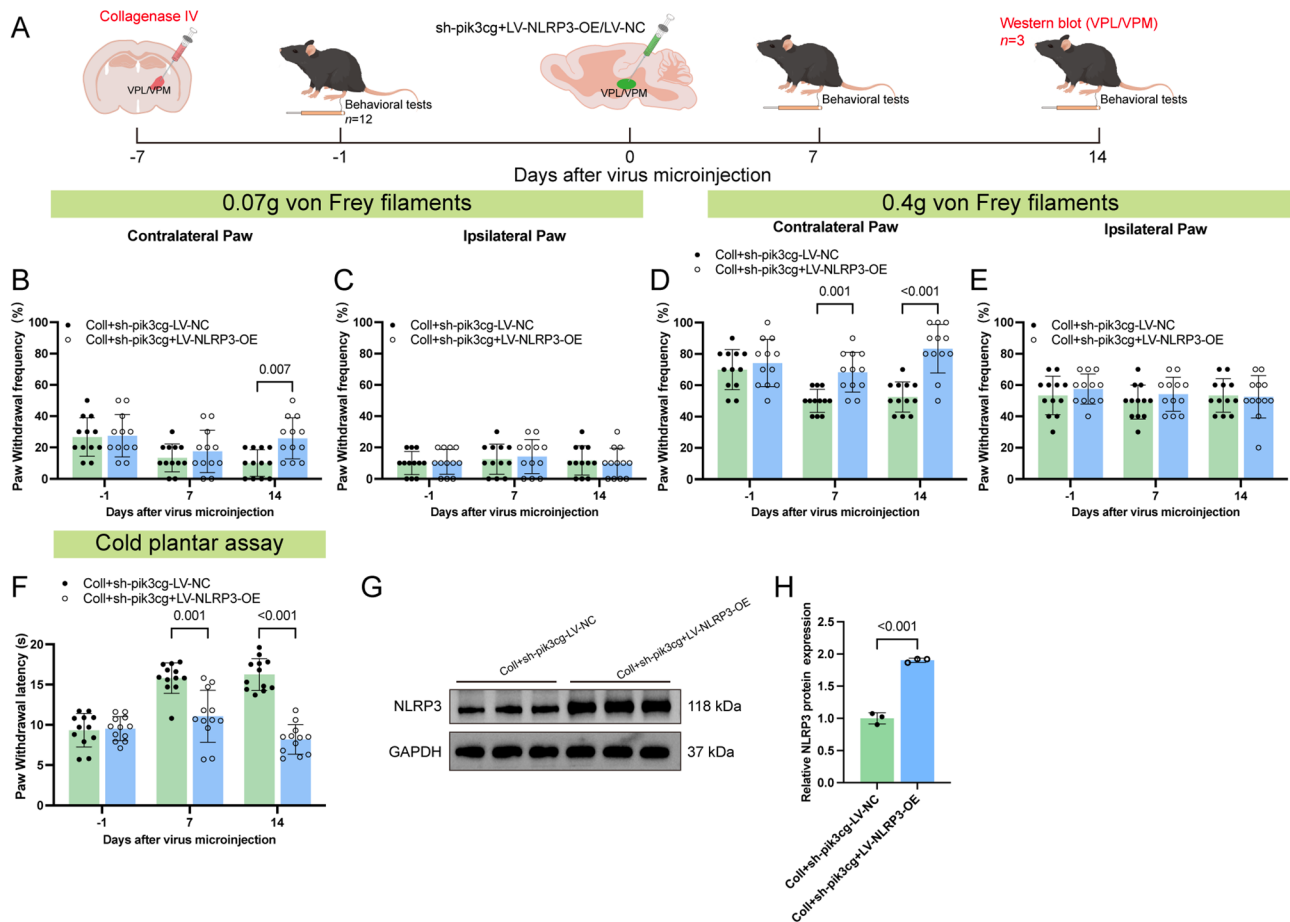


Fig. 9 NLRP3 overexpression counteracted the pain-relieving effects resulting from PIK3CG knockdown. **(A):** Timeline schematic for CPSP model establishment, virus injection, and pain behavior testing time points. **(B–C):** PWF for contralateral **(B)** and ipsilateral **(C)** hind paws in each group, tested using 0.07 g von Frey filaments **(B):** two-way ANOVA followed by Sidak test, $F_{(2,44)}=3.381$, $P=0.04$. **C:** two-way ANOVA followed by Sidak test, $F_{(2,44)}=0.1997$, $P=0.82$; $n=12$. **(D–E):** PWF for contralateral **(D)** and ipsilateral **(E)** hind paws in each group, tested using 0.4 g von Frey filaments **(D):** two-way ANOVA followed by Sidak test, $F_{(2,44)}=6.671$, $P=0.003$. **E:** two-way ANOVA followed by Sidak test, $F_{(2,44)}=0.5016$, $P=0.61$; $n=12$. **(F):** PWL for each group of mice, measured using a 0 °C cold plate (two-way ANOVA followed by Sidak test, $F_{(2,44)}=20.04$, $P<0.001$; $n=12$). **(G):** 14 days after virus injection, NLRP3 protein increased in the Coll + sh-pik3cg + LV-NLRP3-OE group relative to the Coll + sh-pik3cg + LV-NC group (unpaired t -test, $t=16.80$, $df=4$; $n=3$)

that NLRP3 overexpression reverses the analgesic effect induced by PIK3CG knockdown, thereby confirming that NLRP3 functions as a downstream effector of PIK3CG in the regulation of CPSP.

Elevated PIK3CG protein and mRNA levels were observed in the ipsilateral VPL/VPM of the CPSP model. Administration of Danshenol B (50 mg/kg) significantly attenuated mechanical allodynia and cold hyperalgesia, accompanied by reduced PIK3CG expression in the VPL/VPM. Overexpression of PIK3CG counteracted the analgesic effects of Danshenol B, whereas PIK3CG knockdown alleviated pain. Notably, PIK3CG overexpression led to increased NLRP3 levels, while PIK3CG knockdown suppressed NLRP3 expression. Furthermore, the analgesic effect resulting from PIK3CG knockdown was abolished by concurrent NLRP3 overexpression. These findings suggest that Danshenol B alleviates mechanical allodynia and cold hyperalgesia in the CPSP model

by reducing PIK3CG and consequently lowering NLRP3 levels.

Discussion

In this study, we integrated transcriptomic sequencing, network pharmacology, and molecular docking analyses to identify potential therapeutic targets of Danshen and its active components involved in the treatment of CPSP. We demonstrated that oral administration of Danshenol B (50 mg/kg), a key bioactive compound from Danshen, significantly alleviated CPSP symptoms in mice. Mechanistic investigations revealed that Danshenol B exerts its analgesic effect by downregulating the PIK3CG/NLRP3 signaling pathway, which is known to mediate neuroinflammatory processes and chronic pain. These results provide new evidence for the therapeutic value of Danshenol B in CPSP and highlight a novel molecular

mechanism underlying the analgesic effects of traditional Chinese medicine–derived compounds.

We established a CPSP model by injecting collagenase IV into the right VPL/VPM of mice, which led to significant mechanical allodynia and cold hyperalgesia, but not heat hyperalgesia. This finding suggests that the VPL/VPM nuclei may not be critical in transmitting heat pain. Previous studies have implicated the ventral tegmental area–nucleus accumbens circuit in the modulation of thermal nociception [41]; however, no direct evidence has demonstrated the involvement of VPL/VPM in heat pain processing. Consistent with this, functional MRI studies in humans have shown thalamic activation in response to tactile and mechanical stimuli, but not to thermal stimuli [42]. Alternatively, it is possible that the VPL/VPM does contribute to heat pain transmission, but that the key signaling molecules altered in our CPSP model, such as PIK3CG and NLRP3, do not mediate this modality. Supporting this possibility, transcriptomic analysis revealed no significant changes in the expression of known heat pain–related molecules, including Transient Receptor Potential Vanilloid 1 [43] and Regulators of G protein Signaling family members [44].

Transcriptomic sequencing revealed significant alterations in genes related to apoptosis and transcriptional regulation. Previous studies have established that both apoptosis [45] and transcription factors [46] are critically involved in stroke pathophysiology. In the current study, Fig. 4C highlights the central positioning of BTK in the PPI network. BTK is a known regulator of radiation-induced apoptosis [47] and promotes cell death through p53 phosphorylation [48]. These findings suggest that exploring the role of BTK in CPSP through apoptotic mechanisms may offer valuable insights. GO analysis (Supplementary Fig. 4E) identified significant upregulation of *Mmp12* mRNA, which is associated with collagen binding. In addition, both Supplementary Fig. 8 and Fig. 4C underscore the key role of MMP9 within the PPI network, consistent with previous findings in CPSP brain tissue [49]. Matrix metalloproteinases, a family of zinc-dependent endopeptidases, are known to regulate tissue repair [50], inflammation [51], embryonic development [52], angiogenesis [53], and cell migration [54]. Notably, prior studies have demonstrated that reducing MMP2 and MMP9 levels can alleviate mechanical allodynia in CPSP models [49], highlighting MMPs as promising therapeutic targets in post-stroke pain. These genes warrant further experimental validation in future studies.

Numerous studies have investigated Danshen for its analgesic properties. For example, compound Danshen formulations have been shown to relieve both stable [55] and unstable angina [56]. Tanshinone has demonstrated efficacy in models of chemotherapy-induced neuropathic pain [57] and cancer-related bone pain [58]. Additionally,

cryptotanshinone alleviates chronic constriction injury-induced pain through inhibition of the PI3K/Akt signaling pathway [59]. However, the pain-relieving properties of several Danshen-derived components identified in our study—namely MOL007155, tanshinaldehyde, Danshenol B, and sclareol—have not been previously reported. Most existing research on Danshen's analgesic effects has focused on compound formulations or crude extracts, with limited investigation into the roles of individual active constituents in pain management. These findings indicate substantial potential for further exploration of Danshen's individual components in pain therapy.

This study identified a novel analgesic property of Danshenol B. To date, no prior research has reported the use of Danshenol B in the context of pain management. In our study, analgesic effects were observed in mice administered 50 mg/kg of Danshenol B via oral gavage, whereas lower doses of 5 mg/kg and 10 mg/kg did not alleviate pain symptoms. Although higher doses were not tested, it is conceivable that they may further enhance the alleviation of CPSP, potentially accelerating recovery beyond the observed reductions in mechanical allodynia and cold hyperalgesia after 14 days of treatment. Danshenol B is a diterpene compound known to be a potent inhibitor of AR [18]. AR inhibitors are widely recognized for their therapeutic role in managing diabetic peripheral neuropathy [19, 60]. Therefore, we speculate that the analgesic effects of Danshenol B may be attributed, at least in part, to its AR-inhibitory activity.

We identified Danshenol B as a promising therapeutic compound for the treatment of CPSP. Although the candidate compounds were initially selected based on the TCMSP criteria of oral bioavailability $\geq 30\%$ and drug-likeness ≥ 0.183 , Danshenol B demonstrated favorable pharmacokinetic properties. Specifically, it possesses an oral bioavailability of 57.95% and a blood-brain barrier permeability score of 0.1, indicating limited central nervous system penetration. Its transport rate in human colon cancer cells was 0.53 nm/s, suggesting good intestinal absorption. Moreover, its fractional negative accessible surface area (63.59%) implies moderate water solubility, while a topological polar surface area of 0.29 supports adequate membrane permeability. The low number of rotatable bonds (number=2) further suggests a high degree of molecular rigidity and metabolic stability. With a predicted in vivo half-life of 4.27 h, Danshenol B appears suitable for administration 2–3 times daily. Collectively, these parameters support its potential as a drug candidate. In preclinical studies, Danshenol B produced dose-dependent analgesic effects in the CPSP mouse model, with the 50 mg/kg dose demonstrating significant efficacy via oral gavage. However, higher doses were not investigated, and the optimal therapeutic range remains to be determined. Additionally, while no overt

toxicity was observed at the tested dose, the possibility of dose-related toxicity warrants further examination. Future studies should aim to define the compound's safety profile, therapeutic window, and pharmacodynamic characteristics. Moreover, employing drug delivery strategies such as polymer-based carriers may enhance central nervous system penetration and reduce systemic toxicity, thereby improving the clinical translational potential of Danshenol B.

In this study, we demonstrate for the first time that PIK3CG plays a critical role in the pathogenesis of CPSP and that Danshenol B exerts analgesic effects by targeting the PIK3CG/NLRP3 signaling pathway. While previous studies have implicated the PIK3CG/NLRP3 axis in pain regulation in conditions such as arthritis [61] and Complete Freund's Adjuvant-induced neuropathic pain [62], its involvement in CPSP has not been previously reported. Moreover, although network pharmacology analyses have suggested that Danshen may exert anti-tumor effects via the PIK3CG–Akt pathway in ovarian cancer [63], no prior studies have demonstrated that Danshenol B directly regulates PIK3CG or modulates pain through this signaling axis. Our findings provide the first evidence that the PIK3CG/NLRP3 signaling cascade is activated in CPSP and that its inhibition leads to significant analgesic outcomes. Collectively, these results establish a previously unrecognized role for the PIK3CG/NLRP3 signaling axis in CPSP and provide a compelling rationale for targeting PIK3CG in future therapeutic strategies.

Although this study provides compelling preclinical evidence for the involvement of the PIK3CG/NLRP3 signaling pathway in CPSP, its clinical relevance requires further investigation. Notably, elevated PIK3CG levels have been detected in the peripheral blood of stroke patients and are correlated with poor prognosis, suggesting that PIK3CG may serve as a potential therapeutic target for improving post-stroke outcomes [64]. In parallel, NLRP3 has been implicated in a wide range of human disorders, including Alzheimer's disease, Parkinson's disease, and stroke [28]. However, to date, no studies have directly demonstrated the involvement of NLRP3 in human CPSP. Despite this, growing evidence supports a critical role for NLRP3 in human neuropathic pain conditions [65, 66]. Moreover, inhibition of NLRP3 has been shown to alleviate CPSP in rodent models, further reinforcing its potential as a therapeutic target [6]. These observations imply that the PIK3CG/NLRP3 axis may similarly contribute to CPSP pathophysiology in humans. Therefore, our findings provide a mechanistic basis for future clinical studies evaluating this signaling pathway as a potential therapeutic target for post-stroke pain management.

While transcriptomic profiling is a powerful approach for identifying gene expression changes following pharmacological intervention, it may not fully reflect protein-level regulatory mechanisms. In this study, we deliberately chose not to perform RNA sequencing of VPL/VPM tissues from the Coll+Danshenol B and Coll+PBS groups, as our mechanistic focus centered on the regulation of PIK3CG at the protein level. To support this decision, we performed RT-qPCR to examine the mRNA expression of several key genes identified through network pharmacology analysis, including *Btk*, *Casp1*, *Mmp9*, and *Pik3cg* (Supplementary Fig. 10). Notably, none of these genes exhibited significant changes in transcript levels following Danshenol B treatment. This finding suggests that Danshenol B may not exert its effects through transcriptional modulation but rather through post-transcriptional mechanisms, such as altered protein degradation or post-translational modifications. Supporting this notion, our DARTS assay demonstrated that Danshenol B directly binds to PIK3CG and enhances its resistance to proteolytic degradation. Collectively, these results indicate that PIK3CG regulation by Danshenol B likely occurs at the protein level, rather than through changes in mRNA abundance, underscoring the importance of integrating bioinformatic predictions with biochemical validation to elucidate drug mechanisms.

This study has several limitations. First, although molecular docking revealed strong binding affinities, we did not validate whether other active components of Danshen, such as tanshinolone, sclareol, and MOL00715, possess therapeutic potential for CPSP. Second, despite the known AR-inhibitory effect of Danshenol B, we did not investigate whether this mechanism contributes to its analgesic effects in CPSP. Lastly, although Danshenol B exhibited a favorable binding energy with PIK3CG (−9.127 kcal/mol), it did not represent the strongest interaction identified in our docking analysis. The most favorable binding was observed between BTK and MOL007155 (−9.619 kcal/mol). However, due to the unavailability of commercial sources for MOL007155, we synthesized the compound in-house to further investigate its potential interaction with BTK in the context of CPSP.

Conclusions

Our findings revealed that Danshenol B, a component of Danshen, alleviates CPSP by inhibiting the PIK3CG/NLRP3 pathway. These results suggest a potential new clinical application for Danshen extracts in the management of CPSP.

Abbreviations

CPSP	Central post-stroke pain
Danshen	<i>Salvia miltiorrhiza</i>

VPL/MPM	Ventral posterolateral thalamic nucleus and Ventral posteromedial thalamic nucleus
DEGs	Differentially expressed genes
TCM	Traditional Chinese Medicine
PIK3CG	Phosphatidylinositol-4,5-Bisphosphate 3-Kinase Catalytic Subunit Gamma
NLRP3	NLR Family Pyrin Domain Containing 3
mNSS	Modified Neurological Severity Score
PWF	Paw withdrawal frequency
PWL	Paw withdrawal latency
KOG	EuKaryotic Orthologous Groups
GO	Gene Ontology
KEGG	Kyoto Encyclopedia of Genes and Genomes
GSEA	Gene Set Enrichment Analysis
DE	Differentially expressed
BP	Biological Processes
MF	Molecular Functions
CC	Cellular Components
PPI	Protein-protein interaction
Coll	Collagenase IV
MOL007155	Tanshinldehyde and (6 S)-6-(hydroxymethyl)-1,6-dimethyl-8,9-dihydro-7 H-naphtho[8,7-g]benzofuran-10,11-dione
OE	Overexpression
NC	Negative control
GFP	Green fluorescent protein
MMP	Matrix Metalloproteinase
AR	Aldose Reductase

Supplementary Information

The online version contains supplementary material available at <https://doi.org/10.1186/s12967-025-06719-5>.

Supplementary Material 1

Supplementary Material 2

Supplementary Material 3

Acknowledgements

Not applicable.

Author contributions

PL: Conceptualization, Data curation, Funding acquisition, Project administration, Supervision, Visualization. LY: Data curation, Resources, Validation, Visualization, Writing—original draft. JY: Formal analysis, Software, Validation. TZ: Methodology. SZ: Conceptualization, Data curation, Formal analysis, Investigation, Methodology, Project administration, Resources, Software, Supervision, Validation, Visualization, Writing—original draft, Writing—review and editing. All authors read and approved the final manuscript.

Funding

This research was funded by the Henan Province Key Research and Development and Promotion Special Project (Science and Technology Tackling) (grant number: 242102310060 to Panyang Li).

Data availability

The datasets used and/or analysed during the current study are available from the corresponding author on reasonable request. The RNA-seq data were uploaded with Gene Expression Omnibus accession number GSE281041.

Declarations

Ethics approval and consent to participate

All animal care procedures were approved by the Zhengzhou University Animal Care and Use Committee and complied with the International Association for the Study of Pain guidelines. Ethical approval was obtained from the Zhengzhou University Ethics Committee (Approval No. ZZUIRB2024-191).

Declaration of generative AI and AI-assisted technologies in the writing process

During the preparation of this work, the authors used ChatGPT in order to enhance the fluency of the writing and the logical flow of the article. After using this tool, the authors reviewed and edited the content as needed and takes full responsibility for the content of the published article.

Consent for publication

Not applicable.

Competing interests

The authors declare that they have no competing interests.

Author details

¹Department of Human Anatomy, Histology and Embryology, Faculty of Basic Medicine, Henan Medical College, No.8 Shuanghu Avenue, Zhengzhou 451191, China

²Department of Anesthesiology, Henan Provincial Chest Hospital, Affiliated Chest Hospital of Zhengzhou University, Zhengzhou 450000, China

³Department of Human Anatomy, Histology and Embryology, School of Basic Medical Sciences, Zhengzhou University, 100 Science Avenue, Zhengzhou 450001, China

⁴Department of Anesthesiology, Nanfang Hospital, Southern Medical University, No. 1838 North Guangzhou Avenue, Guangzhou 510000, China

⁵Medical Imaging Basic, Department of Medical Technology, Henan Medical College, No.8 Shuanghu Avenue, Zhengzhou 451191, China

Received: 24 February 2025 / Accepted: 5 June 2025

Published online: 23 June 2025

References

1. Klit H, Finnerup NB, Jensen TS. Central post-stroke pain: clinical characteristics, pathophysiology, and management. *Lancet Neurol*. 2009;8:857–68.
2. Mohanan AT, Nithya S, Nomier Y, Hassan DA, Jali AM, Qadri M, Machanchery S. Stroke-Induced central pain: overview of the mechanisms, management, and emerging targets of central Post-Stroke pain. *Pharmaceuticals (Basel)* 2023, 16.
3. Hiraga SI, Itokazu T, Hoshiko M, Takaya H, Nishibe M, Yamashita T. Microglial depletion under thalamic hemorrhage ameliorates mechanical allodynia and suppresses aberrant axonal sprouting. *JCI Insight* 2020, 5.
4. Edwards SA, Ioannou A, Carin-Levy G, Cowey E, Brady M, Morton S, Sande TA, Mead G, Quinn TJ. Properties of pain assessment tools for use in people living with stroke: systematic review. *Front Neurol*. 2020;11:792.
5. JS K. Pharmacological management of central post-stroke pain: a practical guide. *CNS Drugs*. 2014;28:787–97.
6. Shi ZM, Jing JJ, Xue ZJ, Chen WJ, Tang YB, Chen DJ, Qi XY, Huang L, Zou YQ, Wu XZ, Yang F. Stellate ganglion block ameliorated central post-stroke pain with comorbid anxiety and depression through inhibiting HIF-1alpha/NLRP3 signaling following thalamic hemorrhagic stroke. *J Neuroinflammation*. 2023;20:82.
7. Gritsch S, Bali KK, Kuner R, Vardeh D. Functional characterization of a mouse model for central post-stroke pain. *Mol Pain* 2016, 12.
8. XY LZ, FZ L, XT H, HB Z, WK TYSL, XJ Z, GH L. Effect of electroacupuncture on relieving central post-stroke pain by inhibiting autophagy in the hippocampus. *Brain Res*. 2020;1733:146680.
9. Mastroiacovo F, Busceti CL, Biagioni F, Moyanova SG, Meisler MH, Battaglia G, Caricasole A, Bruno V, Nicoletti F. Induction of the Wnt antagonist, Dickkopf-1, contributes to the development of neuronal death in models of brain focal ischemia. *J Cereb Blood Flow Metab*. 2009;29:264–76.
10. Deng L, Zhang J, Chen S, Wu Y, Fan X, Zuo T, Hu Q, Jiang L, Yang S, Dong Z. miR-671-5p upregulation attenuates Blood-Brain barrier disruption in the ischemia stroke model via the NF- κ B, Cyr11cB/MMP-9 signaling pathway. *Mol Neurobiol*. 2023;60:3824–38.
11. Anderson CD, Biffi A, Nalls MA, Devan WJ, Schwab K, Ayres AM, Valant V, Ross OA, Rost NS, Saxena R, et al. Common variants within oxidative phosphorylation genes influence risk of ischemic stroke and intracerebral hemorrhage. *Stroke*. 2013;44:612–9.

12. Hosomi K, Yamamoto T, Agari T, Takeshita S, Tanei T, Imoto H, Mori N, Oshino S, Kurisu K, Kishima H, Saitoh Y. Benefit of spinal cord stimulation for patients with central poststroke pain: a retrospective multicenter study. *J Neurosurg*. 2022;136:601–12.
13. Hamani C, Fonoff ET, Parravano DC, Silva VA, Galhardoni R, Monaco BA, Navarro J, Yeng LT, Teixeira MJ, de Andrade DC. Motor cortex stimulation for chronic neuropathic pain: results of a double-blind randomized study. *Brain*. 2021;144:2994–3004.
14. Sheng R, Chen C, Chen H, Yu P. Repetitive transcranial magnetic stimulation for stroke rehabilitation: insights into the molecular and cellular mechanisms of neuroinflammation. *Front Immunol*. 2023;14:1197422.
15. XD ME, Cao YF, Che YY, Li J, Shang ZP, Zhao WJ, Qiao YJ, Zhang JY. Danshen: a phytochemical and Pharmacological overview. *Chin J Nat Med*. 2019;17:59–80.
16. Collaboration R. Effects of antiplatelet therapy after stroke due to intracerebral haemorrhage (RESTART): a randomised, open-label trial. *Lancet*. 2019;393:2613–23.
17. Sun Y, Yang J. A bioinformatics investigation into the Pharmacological mechanisms of the effect of Fufang Danshen on pain based on methodologies of network Pharmacology. *Sci Rep*. 2019;9:5913.
18. Tezuka Y, Kasimu R, Basnet P, Namba T, Kadota S. Aldose reductase inhibitory constituents of the root of *Salvia miltiorrhiza bunge*. *Chem Pharm Bull (Tokyo)*. 1997;45:1306–11.
19. Chalk C, Benstead TJ, Moore F. Aldose reductase inhibitors for the treatment of diabetic polyneuropathy. *Cochrane Database Syst Rev* 2007, 2007:CD004572.
20. Kaneda MM, Messer KS, Ralainirina N, Li H, Leem CJ, Gorjestani S, Woo G, Nguyen AV, Figueiredo CC, Foubert P, et al. PI3Kgamma is a molecular switch that controls immune suppression. *Nature*. 2016;539:437–42.
21. Luo Q, Raulston EG, Prado MA, Wu X, Gritsman K, Whalen KS, Yan K, Booth CAG, Xu R, van Galen P, et al. Targetable leukaemia dependency on noncanonical PI3Kgamma signalling. *Nature*. 2024;630:198–205.
22. Piddock RE, Loughran N, Marlein CR, Robinson SD, Edwards DR, Yu S, Pillinger GE, Zhou Z, Zaitseva L, Auger MJ, et al. PI3Kdelta and PI3Kgamma isoforms have distinct functions in regulating pro-tumoural signalling in the multiple myeloma microenvironment. *Blood Cancer J*. 2017;7:e539.
23. Jin R, Yu S, Song Z, Quillin JW, Deasis DP, Penninger JM, Nanda A, Granger DN, Li G. Phosphoinositide 3-kinase-gamma expression is upregulated in brain microglia and contributes to ischemia-induced microglial activation in acute experimental stroke. *Biochem Biophys Res Commun*. 2010;399:458–64.
24. Shang S, Liu L, Wu X, Fan F, Hu E, Wang L, Ding Y, Zhang Y, Lu X. Inhibition of PI3Kgamma by AS605240 protects tMCAO mice by attenuating Pro-Inflammatory signaling and cytokine release in reactive astrocytes. *Neuroscience*. 2019;415:107–20.
25. Jin R, Song Z, Yu S, Piazza A, Nanda A, Penninger JM, Granger DN, Li G. Phosphatidylinositol-3-kinase gamma plays a central role in blood-brain barrier dysfunction in acute experimental stroke. *Stroke*. 2011;42:2033–44.
26. Guan X, Fu Q, Xiong B, Song Z, Shu B, Bu H, Xu B, Manyande A, Cao F, Tian Y. Activation of PI3Kgamma/Akt pathway mediates bone cancer pain in rats. *J Neurochem*. 2015;134:590–600.
27. Fu J, Wu H. Structural mechanisms of NLRP3 inflammasome assembly and activation. *Annu Rev Immunol*. 2023;41:301–16.
28. Coll RC, Schroder K, Pelegrin P. NLRP3 and pyroptosis blockers for treating inflammatory diseases. *Trends Pharmacol Sci*. 2022;43:653–68.
29. Xia CY, Guo YX, Lian WW, Yan Y, Ma BZ, Cheng YC, Xu JK, He J, Zhang WK. The NLRP3 inflammasome in depression: potential mechanisms and therapies. *Pharmacol Res*. 2023;187:106625.
30. Li JM, Deng HS, Yao YD, Wang WT, Hu JQ, Dong Y, Wang PX, Liu L, Liu ZQ, Xie Y, et al. Sinomenine ameliorates collagen-induced arthritis in mice by targeting GBP5 and regulating the P2X7 receptor to suppress NLRP3-related signaling pathways. *Acta Pharmacol Sin*. 2023;44:2504–24.
31. Takahashi M. NLRP3 inflammasome as a key driver of vascular disease. *Cardiovasc Res*. 2022;118:372–85.
32. Li W, Shen N, Kong L, Huang H, Wang X, Zhang Y, Wang G, Xu P, Hu W. STING mediates microglial pyroptosis via interaction with NLRP3 in cerebral ischaemic stroke. *Stroke Vasc Neurol*. 2024;9:153–64.
33. Tao YW, Yang L, Chen SY, Zhang Y, Zeng Y, Wu JS, Meng XL. Pivotal regulatory roles of traditional Chinese medicine in ischemic stroke via inhibition of NLRP3 inflammasome. *J Ethnopharmacol*. 2022;294:115316.
34. Schallert T, Kozlowski DA, Humm JL, Cocke RR. Use-dependent structural events in recovery of function. *Adv Neurol*. 1997;73:229–38.
35. Su S, Yudin Y, Kim N, Tao YX, Rohacs T. TRPM3 channels play roles in heat hypersensitivity and spontaneous pain after nerve injury. *J Neurosci*. 2021;41:2457–74.
36. Cunningham CB, Benowitz KM, Moore AJ. The updated genome of the burying beetle *Nicrophorus vespilloides*, a model species for evolutionary and genetic studies of parental care. *Ecol Evol*. 2024;14:e70601.
37. Love MI, Huber W, Anders S. Moderated Estimation of fold change and dispersion for RNA-seq data with DESeq2. *Genome Biol*. 2014;15:550.
38. Liao Y, Smyth GK, Shi W. FeatureCounts: an efficient general purpose program for assigning sequence reads to genomic features. *Bioinformatics*. 2014;30:923–30.
39. Cozzini P, Fornabaio M, Marabotti A, Abraham DJ, Kellogg GE, Mozzarelli A. Simple, intuitive calculations of free energy of binding for protein-ligand complexes. 1. Models without explicit constrained water. *J Med Chem*. 2002;45:2469–83.
40. Lu C, Liu J, Escames G, Yang Y, Wu X, Liu Q, Chen J, Song Y, Wang Z, Deng C, et al. PI3Kγ regulates NLRP3/GSDMD-Mediated pyroptosis in septic myocardial injury. *Inflammation*. 2023;46:2416–32.
41. Zhang H, Qian YL, Li C, Liu D, Wang L, Wang XY, Liu MJ, Liu H, Zhang S, Guo XY, et al. Brain-Derived neurotrophic factor in the mesolimbic reward circuitry mediates nociception in chronic neuropathic pain. *Biol Psychiatry*. 2017;82:608–18.
42. Habig K, Kramer HH, Lautenschlager G, Walter B, Best C. Processing of sensory, painful and vestibular stimuli in the thalamus. *Brain Struct Funct*. 2023;228:433–47.
43. Iftinca M, Defaye M, Altier C. TRPV1-Targeted drugs in development for human pain conditions. *Drugs*. 2021;81:7–27.
44. Bosier B, Doyen PJ, Brolet A, Muccioli GG, Ahmed E, Desmet N, Hermans E, Deumens R. Inhibition of the regulator of G protein signalling RGS4 in the spinal cord decreases neuropathic hyperalgesia and restores cannabinoid CB1 receptor signalling. *Br J Pharmacol*. 2015;172:5333–46.
45. Chen X, Li Z, Zhang B, Liu T, Yao W, Wan L, Zhang C, Zhang Y. Antinociception role of 14,15-epoxyicosatrienoic acid in a central post-stroke pain model in rats mediated by anti-inflammation and anti-apoptosis effect. *Neurochem Int*. 2022;154:105291.
46. Yang F, Luo WJ, Sun W, Wang Y, Wang JL, Yang F, Li CL, Wei N, Wang XL, Guan SM, Chen J. SDF1-CXCR4 signaling maintains central Post-Stroke pain through mediation of Glial-Neuronal interactions. *Front Mol Neurosci*. 2017;10:226.
47. Uckun FM, Waddick KG, Mahajan S, Jun X, Takata M, Bolen J, Kurosaki T. BTK as a mediator of radiation-induced apoptosis in DT-40 lymphoma B cells. *Science*. 1996;273:1096–100.
48. Althubiti M, Rada M, Samuel J, Escorsa JM, Najeeb H, Lee KG, Lam KP, Jones GD, Barlev NA, Macip S. BTK modulates p53 activity to enhance apoptotic and senescent responses. *Cancer Res*. 2016;76:5405–14.
49. Bai Q, Han Y, Khan S, Wu T, Yang Y, Wang Y, Tang H, Li Q, Jiang W, editors. A Novel Endoplasmic Reticulum-Targeted Metal-Organic Framework-Confined Ruthenium (Ru) Nanozyme Regulation of Oxidative Stress for Central Post-Stroke Pain. *Adv Healthc Mater* 2024, 13:e2302526.
50. Chang M. Matrix metalloproteinase profiling and their roles in disease. *RSC Adv*. 2023;13:6304–16.
51. Lee HS, Kim WJ. The role of matrix metalloproteinase in inflammation with a focus on infectious diseases. *Int J Mol Sci* 2022, 23.
52. Zhang L, Li Y, Guan CY, Tian S, Lv XD, Li JH, Ma X, Xia HF. Therapeutic effect of human umbilical cord-derived mesenchymal stem cells on injured rat endometrium during its chronic phase. *Stem Cell Res Ther*. 2018;9:36.
53. Fields GB. Mechanisms of action of novel drugs targeting Angiogenesis-Promoting matrix metalloproteinases. *Front Immunol*. 2019;10:1278.
54. Kurt-Celep I, Nihan Kilinc A, Griffin M, Telci D. Nitrosylation of tissue transglutaminase enhances fibroblast migration and regulates MMP activation. *Matrix Biol*. 2022;105:1–16.
55. Zhang GX, Zhang YY, Zhang XX, Wang PQ, Liu J, Liu Q, Wang Z. Different network Pharmacology mechanisms of Danshen-based Fangjis in the treatment of stable angina. *Acta Pharmacol Sin*. 2018;39:952–60.
56. Wu JR, Liu S, Zhang XM, Zhang B. Danshen injection as adjuvant treatment for unstable angina pectoris: A systematic review and meta-analysis. *Chin J Integr Med*. 2017;23:306–11.
57. Di Cesare Mannelli L, Piccolo M, Maione F, Ferraro MG, Irace C, De Feo V, Ghelardini C, Mascolo N. Tanshinones from *Salvia miltiorrhiza bunge* revert chemotherapy-induced neuropathic pain and reduce glioblastoma cells malignancy. *Biomed Pharmacother*. 2018;105:1042–9.

58. Hao W, Chen L, Wu LF, Yang F, Niu JX, Kaye AD, Xu SY. Tanshinone IIA exerts an antinociceptive effect in rats with Cancer-induced bone pain. *Pain Physician*. 2016;19:465–76.
59. Zhang W, Suo M, Yu G, Zhang M. Antinociceptive and anti-inflammatory effects of Cryptotanshinone through PI3K/Akt signaling pathway in a rat model of neuropathic pain. *Chem Biol Interact*. 2019;305:127–33.
60. Airey M, Bennett C, Nicolucci A, Williams R. Aldose reductase inhibitors for the prevention and treatment of diabetic peripheral neuropathy. *Cochrane Database Syst Rev* 2000, 1996:CD002182.
61. Xu B, Xu Y, Kong J, Liu Y, Zhang L, Shen F, Wang J, Shen X, Chen H. Chrysin mitigated neuropathic pain and peripheral sensitization in knee osteoarthritis rats by repressing the RAGE/PI3K/AKT pathway regulated by HMGB1. *Cytokine*. 2024;180:156635.
62. Zhou M, Tan W, Hasimu H, Liu J, Gu Z, Zhao J. Euphorbium total triterpenes improve Freund's complete adjuvant-induced arthritis through PI3K/AKT/Bax and NF-kappaB/NLRP3 signaling pathways. *J Ethnopharmacol*. 2023;306:116146.
63. Xu X, Zhang Z, Liu L, Che C, Li W. Exploring the Antiovarian Cancer Mechanisms of *Salvia Miltiorrhiza* Bunge by Network Pharmacological Analysis and Molecular Docking. *Comput Math Methods Med* 2022, 2022:7895246.
64. Amini H, Knepp B, Rodriguez F, Jickling GC, Hull H, Carmona-Mora P, Bushnell C, Ander BP, Sharp FR, Stamova B. Early peripheral blood gene expression associated with good and poor 90-day ischemic stroke outcomes. *J Neuroinflammation*. 2023;20:13.
65. Chen R, Yin C, Fang J, Liu B. The NLRP3 inflammasome: an emerging therapeutic target for chronic pain. *J Neuroinflammation*. 2021;18:84.
66. Starobova H, Nadar EI, Vetter I. The NLRP3 inflammasome: role and therapeutic potential in pain treatment. *Front Physiol*. 2020;11:1016.

Publisher's note

Springer Nature remains neutral with regard to jurisdictional claims in published maps and institutional affiliations.